Myogenesis modelled by human pluripotent stem cells uncovers Duchenne muscular dystrophy phenotypes prior to skeletal muscle commitment

Virginie Mournetas[1*], Emmanuelle Massouridès[2], Jean-Baptiste Dupont[1], Etienne Kornobis[3], Hélène Polvèche[2], Margot Jarrige[2], Maxime R. F. Gosselin[4]; Antigoni Manousopoulou[5], Spiros D. Garbis[6]; Dariusz C. Górecki[4,7]; Christian Pinset[8]

[*] Correspondence: vmournetas@istem.fr

[1]INSERM UEVE UMR861, I-STEM, AFM, 28 rue Henri Desbruères, 91100 Corbeil-Essonnes, France

[2]CECS, I-STEM, AFM, 28 rue Henri Desbruères, 91100 Corbeil-Essonnes, France

[3]Institut Pasteur, 25-28 Rue du Dr Roux, 75015 Paris, France

[4]Molecular Medicine, School of Pharmacy and Biomedical Sciences, University of Portsmouth, PO1 2DT, Portsmouth, UK

[5]Department of Immuno-Oncology, Beckman Research Institute, City of Hope National Medical Center, Duarte, CA, 91010, USA

[6]Proteome Exploration Laboratory, Beckman Institute, California Institute of Technology, Division of Biology and Biological Engineering, 1200 E. California Blvd., MC 139-74, Pasadena, California, 91125, USA

[7]Military Institute of Hygiene and Epidemiology, Warsaw, Poland

[8]CNRS, I-STEM, AFM, 28 rue Henri Desbruères, 91100 Corbeil-Essonnes, France

ABSTRACT

Duchenne muscular dystrophy (DMD) causes severe disability of children and death of young men, with an incidence of approximately 1/5,000 male births. Symptoms appear in early childhood, with a diagnosis made around 4 years old, a time where the amount of muscle damage is already significant, preventing early therapeutic interventions that could be more efficient at halting disease progression. In the meantime, the precise moment at which disease phenotypes arise – even asymptomatically – is still unknown. Thus, there is a critical need to better define DMD onset as well as its first manifestations, which could help identify early disease biomarkers and novel therapeutic targets.

In this study, we have used human induced pluripotent stem cells (hiPSCs) from DMD patients to model skeletal myogenesis, and compared their differentiation dynamics to healthy control cells by a comprehensive multi-omics analysis. Transcriptome and miRnome comparisons combined with protein analyses at 7 time points demonstrate that hiPSC differentiation 1) mimics described DMD phenotypes at the differentiation endpoint; and 2) homogeneously and robustly recapitulates key developmental steps - mesoderm, somite, skeletal muscle - which offers the possibility to explore dystrophin functions and find earlier disease biomarkers.

Starting at the somite stage, mitochondrial gene dysregulations escalate during differentiation. We also describe fibrosis as an intrinsic feature of skeletal muscle cells that starts early during myogenesis. In sum, our data strongly argue for an early developmental manifestation of DMD whose onset is triggered before the entry into the skeletal muscle compartment, data leading to a necessary reconsideration of dystrophin functions during muscle development.

INTRODUCTION

Duchenne muscular dystrophy (DMD) is a rare genetic disease, but it is the most common form of myopathy affecting approximately one in 5,000 male births and very rarely female. In this recessive X-linked monogenic disorder, mutations in the DMD gene lead to the loss of a functional dystrophin protein, resulting in a progressive - yet severe - muscle wasting phenotype (1). In patients, symptoms usually appear in early childhood (2-5 years old) and worsen with age, imposing the use of wheelchair before 15 and leading to premature death by cardiac and/or respiratory failure(s) mostly around 30 years of age (2).

At the age of diagnosis, around 4 years old, muscles of DMD patients have already suffered from the pathology (3,4). Several reviews pointed out the limitations of current disease biomarkers, which fail to detect the development of DMD specifically and at an early age (5,6). Meanwhile, no treatment is available to stop this degenerative disease yet. Developing therapies aim at restoring the expression of dystrophin in muscle cells but, so far, the level stays too low to be beneficial to patients (7). The absence of both reliable biomarkers and effective therapies stress the need of better defining the first steps of DMD in Human to be able to 1) find specific markers of disease initiation in order to increase diagnosis sensitivity and, therefore, improve patient management by accelerating their access to better healthcare; and 2) develop alternative therapeutic approaches by finding targets that compensate the lack of dystrophin and complement current attempts at restoring its expression (8).

In 2007, a seminal publication reported that the gene expression profile of muscles from asymptomatic DMD children younger than 2 years old is already distinguishable from healthy muscles, suggesting that DMD molecular dysregulations appear before disease symptomatic manifestations (4). Evidence obtained in multiple animal models, such as neonatal *GRMD* dogs (9), DMD zebrafish (10) and *mdx* mouse embryos (11), as well as in human foetuses (12–14) even suggest that DMD starts before birth, during prenatal development. Our team recently identified the embryonic dystrophin isoform Dp412e expressed in early mesoderm-committed cells (15), another indication that DMD can start *in utero*. Further exploring DMD onset in human foetuses is extremely challenging for obvious ethical and practical reasons. A way to overcome these issues is to develop a human DMD model *in vitro*, recapitulating embryonic development from human pluripotent stem cells to skeletal muscle lineages.

To our knowledge, none of the existing human DMD *in vitro* models, either based on tissue-derived myoblasts (16) or on the differentiation of induced pluripotent stem cells (17–21), have been used for studying DMD during the ontogeny of the skeletal muscle lineage. Moreover, original protocols for *in vitro* myogenesis from human pluripotent stem cells (reviewed in (22)) use transgene overexpression or/and cell sorting procedures, and thereby, miss the steps preceding skeletal muscle commitment, *e.g.* paraxial mesoderm and myotome. Novel protocols have recently used transgene-free directed differentiation to recapitulate human embryonic development in a dish, giving theoretical access to the developmental steps (19,23–25).

In the present study, we compared the myogenic differentiation dynamics of healthy and DMD hiPSCs using a multi-omic approach to identify early disease manifestations *in vitro*. DMD cells showed marked transcriptome dysregulations from day 10, before the detection of skeletal muscle regulatory factors at day 17. Specifically, we identified the dysregulation of mitochondrial genes as one of the earliest detectable phenotypes. These alterations escalated over the course of muscle specification. In addition, we showed an early induction of Sonic hedgehog signalling pathway, followed by collagens as well as fibrosis-related genes suggesting the existence of an intrinsic fibrotic process solely driven by DMD muscle cells. Overall, our data highlight that human pluripotent stem cells are a suitable cell model to study muscle development in both healthy and disease conditions. In the context of DMD, they strongly argue for the existence of early disease manifestations during somite development.

RESULTS

To establish the early/developmental impact of *DMD* gene mutations, human induced pluripotent stem cells (hiPSCs) from three DMD patients and three healthy individuals were generated as described previously (15). These cells, when subjected to a standardised differentiation protocol without utilisation of feeder cells, cell sorting or gene overexpression, formed elongated and plurinucleated myotubes within 25 days (23), with an amplification fold of 2918 ± 480 (mean ± SEM). Skeletal muscle progenitor cells after 17 days of differentiation could be cryopreserved (Figure S1A). Whole transcriptome and miRnome profiles were compared at 7 differentiation time points (tissue-derived myoblasts and myotubes, as well as hiPSC-derived cells at days 0, 3, 10, 17 and 25) and complemented by TMT proteomics and Western blot analyses (Table S1).

DMD is initiated prior to the expression of skeletal muscle markers

First, the expression profile of the *DMD* variants was studied by RT-qPCR in healthy and DMD hiPSCs during the differentiation process described in Figure S1A. The *Dp427m* variant, which is normally observed in muscle cells (26), appeared from day 17, in contrast with *Dp412e* – the embryonic variant of dystrophin present in mesoderm cells (15) – which was expressed at differentiation day 3. Therefore, the expression of the *DMD* locus is initiated in the very first steps of our differentiation protocol, well before myotube formation. The ubiquitous variant *Dp71-40* was detected at every time points, in contrast with *Dp116* (Schwann cell variant (27)), *Dp140* (kidney and foetal brain variant (28)) and *Dp427p1p2* (Purkinje cell variant (29)), which were all undetected at the examined time points (Figure S1B). Interestingly, *Dp260* (retinal variant (30)) followed a similar expression pattern than *Dp427m*. *Dp427c* (cerebral variant (31)) was also detected at days 17 and 25, but at a very low level. As expected, DMD cells expressed lower levels of *Dp427m* and *Dp260* (Figure S1B).

A strong correlation in the transcriptomic data was observed by mRNA-seq and miRNA-seq between samples collected at an individual time point, as opposed to samples from two distinct time points. In addition, the correlation coefficient between samples taken at two successive time points increased as differentiation progressed (Figure 1A). Differential expression analysis between two successive collection days (days 3/0, days 10/3, days 17/10, days 25/17) in healthy controls showed that the proportion of regulated genes decreased from 20 % to 12 % of the whole transcriptome (2223 to 1284 mRNAs, adjusted pvalue ≤ 0.01) through the course of differentiation. These observations demonstrate the robustness of the differentiation protocol and are in agreement with an early specialisation and a later refinement of the transcriptome as cells quickly exit pluripotency and become progressively restricted to the skeletal muscle lineage.

To characterise the developmental stages achieved by the cells, the expression of lineage-specific markers (both mRNAs and miRNAs) was determined at each time point, together with gene enrichment analyses (Figure 1B-2A, Figure S2B-C, Table S2).

Pluripotency was similarly maintained in healthy and DMD cells at day 0 (Figure 2A, Table S2), as already shown by our group (15). At day 3, cells lost pluripotency and became paraxial mesoderm cells expressing marker genes such as *PAX3* and *PAX7* (11) (Figure 2A, Table S2). Importantly, markers of lateral plate (*e.g. GATA4* (32)) and intermediate mesoderm (*e.g. PAX8* (33)) were not upregulated at this stage (Table S2).

Similarly, earlier markers of primitive streak (*e.g. TBX6* (34)), mesendoderm (*e.g. MIXL1* (35)), as well as markers of the other germ layers, endoderm (*e.g. SOX17* (36)) and ectoderm (*e.g. SOX2* (37)) were either not expressed, greatly downregulated or expressed at very low levels (Table S2), suggesting cell homogeneity in the differentiation process.

At that early time point, DMD-associated gene dysregulation represented less than 3 % of the entire transcriptome (adjusted pvalue ≤ 0.05, Figure 2B) but already contained genes important for development (*e.g. MEIS2* (38)) and muscle formation (*e.g. ACTA1* (39)). However, mesoderm markers were not significantly dysregulated, attesting that mesoderm commitment was mostly unimpaired (Figure 2A, Table S2). No increase in the expression of primitive streak, mesendoderm, endoderm or ectoderm markers was detected, suggesting no differences in the differentiation process of DMD cells at that stage (Table S2).

In contrast, a sharp increase in the proportion of dysregulated genes appeared at day 10 compared to day 0 and day 3, mostly including gene downregulations (DMD/Healthy expression ratio ≤ 0.76, adjusted pvalue ≤ 0.05). This concerned almost 10 % of the transcriptome at day 10 (against 3 % at day 3) and remained stable from 10 to 12 % (1226 mRNAs) until day 25 (Figure 2B). At day 10, healthy cells started to express genes typically observed during somitogenesis, such as *PAX3* (40) *NR2F2* (41), *PTN* (42), *MET* (43), *H19* and *IGF2* (44) (Table S2). More precisely, their transcriptome exhibits a mixed profile between dermomyotome (expression of *GLI3* (45) and *GAS1* (46) but not *ZIC3* (47)) and myotome (expression of *MET* (48) and *EPHA4* (49) but not *LBX1* (50)) (Table S2). Neither markers of presomitic mesoderm cells (*e.g. FGF8* (51)) and neural plate cells (*FOXD3* (52)), nor markers of sclerotome (*e.g. PAX1* (53)) and dermatome (*e.g. EGFL6* (54)) were upregulated (Table S2). In DMD cells, no increase of presomitic mesoderm, neural plate, sclerotome or dermatome markers was observed (Table S2). In the meantime, several somite markers were downregulated, including *H19, IGF2*, *MET* and *SEMA6A* (55) (validated at the protein level for SEMA6A, Figure 2A-S3A, Table S2), while a slight upregulation of chondrocyte markers was highlighted and confirmed at the protein level for GLI3 (Figure S3B), together with a significant enrichment of the gene ontology term ‘nervous system development’, suggesting potential lineage bifurcations at day 10 (Figure 2A-S2C, Table S2).

The study of differentiation dynamics presented above highlights that mesoderm commitment is not impaired by the absence of dystrophin, and shows that DMD onset takes place at the somite cell stage, before the

146 expression of the skeletal muscle program and especially before the expression of *Dp427m*, the muscle variant
147 of the *DMD* gene.

148 **DMD hiPSC can become skeletal muscle progenitor cells, but exhibit specific muscle gene dysregulations**

149 Healthy and DMD cells were in the skeletal muscle compartment at day 17, as evidenced by the expression of
150 multiple lineage-specific genes and proteins, such as transcription factors (*e.g. MYOD1* (56)), cell surface
151 markers (*e.g. CDH15* (57)), sarcomere genes (*e.g. TNNC2* (58)), dystrophin-associated protein complex (DAPC)
152 genes (*e.g. SGCA* (59)), Calcium homeostasis genes (*e.g. RYR1* (60)) and muscle-specific miRNAs (myomiR, *e.g.*
153 *MIR1-1* (61)), (Figure 1B, Table S2). They both showed an embryonic/foetal phenotype characterised by *ERBB3*
154 expression, in contrast with tissue-derived myoblasts that expressed *NGFR* (21). Here again, alternative cell
155 lineages were absent or greatly downregulated, such as tenocytes (*e.g. MKX* (62)), chondrocytes (*e.g. SOX5*
156 (63)), osteoblasts (*e.g. SPP1* (64)) or nephron progenitors (*e.g. SALL1* (65)) (Table S2).
157 Interestingly, DMD cells did not show dysregulated expression of skeletal muscle transcription factors (Table
158 S2). However, several myomiRs were found downregulated (*e.g. MIR1-1*, Figure 2C), together with genes
159 related to calcium homeostasis (*e.g. ATP2A2* (66), at both mRNA and protein level, Figure 2D-E) as well as
160 members of the DAPC (*e.g. SNTA1* (67)) (Table S2). Concerning cell lineages, there was no visible difference
161 when compared to healthy controls, except an upregulation of markers associated with chondrocytes, which
162 was confirmed at the protein level for GLI3 (Figure S3C), and a significant enrichment of the gene ontology
163 term 'nervous system development' previously seen at day 10, together with 'kidney development' and
164 'ossification' (Figure 2A-S2C, Table S2).
165 Therefore, DMD cells efficiently enter the skeletal muscle compartment at day 17, but exhibit dysregulations in
166 several features typically associated with dystrophic muscles, which could be a direct consequence of the early
167 manifestations of DMD detected at day 10.

168 **hiPSC differentiation lead to embryonic/foetal myotubes that reproduce DMD phenotypes**

169 As previously described (23), both healthy and DMD hiPSC-derived myotubes (day 25) were able to twitch
170 spontaneously in culture, and fluorescent staining of nuclei and α-actinin confirmed cell fusion and the
171 formation of striation patterns typical of muscle fibres *in vivo* (Figure 3A). Western blot analyses on protein

extracts from DMD cells confirmed that dystrophin was either undetectable or slightly expressed (Figure 3B), as in the corresponding patient muscle biopsies.

We selected representative mRNAs and miRNAs and showed that both hiPSC-derived and tissue-derived myotubes have exited the cell cycle and upregulated genes expressed in skeletal muscles (Figure S4A, Figure 4A, Table S2). This included skeletal muscle myomiRs (*MIR1-1*, *MIR133* and *MIR206* (68,69)), transcription factors involved in skeletal myogenesis including those of the MRF family (*e.g. MYOD1* (56), *MYOG* (70)), specific muscle cell surface markers (*e.g. CDH15* (57), *ITGA7* (71)) as well as genes involved in the formation of the DAPC (*e.g. SGCA* (59), *DTNA* (72)), sarcomeres (*e.g. TNNC2* (58), *TNNT3* (73)), myofibril organisation (*e.g. UNC45B* (74), *NACA* (75)) and the execution of excitation-contraction coupling at the neuromuscular junction (NMJ, *e.g. MUSK* (76), *DOK7* (77)) (Figure 4A, Table S2).

Even though global analysis showed that hiPSC-derived myotubes were similar to their tissue-derived counterparts in term of lineage commitment, they displayed an embryonic/foetal phenotype – as suggested in progenitors at day 17. This can be illustrated by the expression of the embryonic/foetal myosin heavy/light chains *MYH3* (78), *MYH8*(79), *MYL4* (80) and *MYL5* (81) but not the postnatal transcripts *MYH1* and *MYH2* (82), which were detected in tissue-derived myotubes. Myotubes derived from hiPSCs had also higher levels of *IGF2*, which is downregulated at birth (83), and expressed *DLK1*, which is known to be extinct in adult muscles (84) (Figure S4B).

Despite the embryonic/foetal phenotype, hiPSC-derived myotubes showed evidence of terminal differentiation and cellular maturation. First, their total level of myosin heavy chain proteins was significantly higher than in tissue-derived myotubes, as confirmed by Western blotting (Figure 3B). RNAs and proteins involved in DAPC formation (*e.g.* DMD, SGCA (59) and SGCG (85)), as well as in excitation-contraction coupling (*e.g.* RYR1 (60) and CACNA1S / CAV1.1 (86)) were also present at higher levels (Figure 3B-4A). Finally, higher expression of skeletal muscle transcription factors (*e.g. MEF2C* (87)), and of multiple genes involved in muscle contraction (*e.g. TNNT3* (73)), NMJ formation (*e.g. RAPSN* (88)), and creatine metabolism (*e.g. CKM* (89)) indicates that hiPSC-derived cells expressed features of fully differentiated muscle cells (Figure 4A). Similar to previous time points, day 25 cells were negative for markers of alternative muscle lineages, *i.e.* cardiac (*MIR208a* (90), *MYL7* (91) and *RYR2* (92)) and smooth muscle cells (*MYH11* (93), *CNN1* (94) and *CHRNA3/B2/B4* (95)).

In DMD cells, there was a global trend toward downregulation of muscle transcription factors, which was only significant for *MEF2A* and *MEF2D* in hiPSC-derived myotubes and *EYA4* and *MYOD1* in tissue-derived myotubes (Figure S4C). In addition, myomiRs previously associated with muscle dystrophy (dystromiRs, *e.g. MIR1-1* (61), Figure 2C) were found downregulated (Table S2). Similarly, a global downregulation phenotype was observed in both tissue- and hiPSC-derived DMD myotubes, and concerned multiple genes associated with known disease phenotypes, such as cell surface markers (*e.g. ITGA7* (71)), DAPC organisation (*e.g. SGCA* (59)), myofibril organisation (*e.g. UNC45B* (74)), sarcomere formation (*e.g. MYO18B* (96)), NMJ function (*e.g. CHRNB1* (97)) and calcium homeostasis (*e.g. ATP2A2* (66), Figure 2D, 4B, S2C).

Altogether, these data indicate that hiPSC-derived myotubes recapitulate a full skeletal muscle differentiation program, and exhibit an embryonic/foetal phenotype. Despite that, it shows that disease phenotypes usually observed in young adult animal models are detectable at least at the transcriptional level which validates the quality of this cell system to model the DMD pathology.

Fibrosis, an intrinsic feature of DMD cells independent of TGF-β pathway

As presented above, the upregulation of chondrocyte markers in DMD cells, although already present at day 10, became significant from day 17 (Figure 2A, Table S2). It was accompanied by the upregulations of the Sonic hedgehog (SHH) signalling pathway and of multiple collagens (Figure 5A, Table S2). Genes encoding the *P4H* collagen synthases, were not dysregulated while *RRBP1* (that stimulates collagen synthesis (98)) together with *PLOD1* and *PLOD2* (that stabilise collagens (99,100)) were significantly upregulated. Moreover, *SETD7*, a gene known for activating collagenases (101), was significantly downregulated.

At the myotube stage, a fibrosis-related gene set was clearly upregulated in DMD cells, as illustrated by the overexpression of *ANGPT1* (102), *CTGF* (103), collagens (*e.g. COL1A2* (104)), matrix metallopeptidases (*MMPs*) and tissue inhibitors of metallopeptidase (*TIMPs*) (105) (Figure 5B). Conversely, the myomiR *MIR133* that controls *CTGF* expression (106) was repressed (Table S2). Interestingly, gene members of the transforming growth factor (TGF)-β pathway, a well-known inducer of fibrosis (107), were not found dysregulated (Figure 5B, Table S2).

Altogether, these data argue for fibrosis as an intrinsic feature of DMD skeletal muscle cells, rather than a process solely driven by interstitial cell populations in the niche. Furthermore, this muscle-driven fibrosis

seems independent of the TGF-β pathway, and could rather depend on the SHH pathway, together with an intrinsic upregulation of chondrocyte markers and collagens.

Mitochondria, a key organelle impacted by the absence of dystrophin prior calcium dysregulation

As previously described (108) and illustrated on Figure S5A, the energy metabolism of DMD hiPSC-derived myotubes was dysregulated at the creatine and carbohydrate levels, up to the respiration (Figure 6A-B, Figure S2C, Table S2). The creatine transporter was not impacted while mRNAs coding for enzymes of both creatine and creatine phosphate biosynthesis were underrepresented. Neither glucose nor glutamate transporter expression were impaired. However, glutamine biosynthesis (followed by gluconeogenesis that feeds glycolysis from glutamine) as well as glycogenesis (followed by glycogenolysis that feeds glycolysis from glycogen) were all downregulated, together with glycolysis itself. In contrast, the pentose phosphate pathway, which is in parallel to glycolysis, was upregulated, especially the oxidative part. Pyruvate decarboxylation and generation of acetyl-CoA to feed the tricarboxylic acid (TCA) cycle was also impaired. Finally, the TCA cycle itself (Figure 6A, Figure S2C) and the mitochondrial electron transport chain were downregulated Figure 6B, Figure S2C). This is particularly reinforced by lower levels of a member of the ATP synthase complex ATP5A1 at both mRNA and protein levels (Figure 6C-D). Moreover, transcripts encoded by the mitochondrial DNA and mitochondrial DNA itself were decreased in DMD hiPSC-derived myotubes at day 25 (Figure S5B-S5E).

In the presented cell model, a significant downregulation of a mRNA set coding for mitochondrial proteins was primarily observed at day 10 with the downregulation of 11 % (12 mRNAs, DMD/Healthy expression ratio ≤ 0.76, adjusted pvalue ≤ 0.05) of the mitochondrial outer membrane genes, and amplified during the differentiation of DMD cells (Figure 7A). Therefore, defects depicted at day 25 rooted before the expression of the skeletal muscle program at day 17. Among them, mRNA downregulation of *TSPO*, a channel-like molecule involved in the modulation of mitochondrial transition pore (109), occurred from day 10 to day 25. This downregulation was also observed at the protein level at day 17 (Figure 7B). Moreover, the protein import system was affected from day 17 at both mRNA and protein levels (Figure S5C-S5F). Simultaneously, mRNAs involved in mitochondrial genome transcription started to be downregulated, followed by genes involved in mitochondrial DNA replication at day 25 (Figure S5D-S5G). This progressive increase of dysregulations was also observed at the level of the entire mRNA set related to mitochondria (around 1,000 mRNAs) as illustrated by the volcano plots as well as the gene ontology enrichments (Figure 7C, Figure S2C).

Our data highlight early impairments in genes coding for mitochondria that start at the somite stage - prior calcium homeostasis dysregulation - and increase with the differentiation in an orderly manner. These elements complete the mitochondrial DMD phenotype described above at the myotube stage.

Altogether, our study demonstrates that DMD starts prior to the expression of well-described markers of muscle differentiation. It shows that hiPSC-based experimental models of DMD can help identify early disease manifestations and stratify multiple pathological features over the course of muscle development.

DISCUSSION

Since the discovery of the *DMD* gene in 1987 (1), DMD cellular phenotypes were considered under the unique scope of a “mechanical hypothesis” in which dystrophin deficiency led to membrane leakage and ultimately muscle cell rupture. However, over the last 15-20 years, studies have brought unequivocal evidence that multiple additional factors are in play, such as calcium intracellular overloads (110,111), excessive oxidative stress (112,113), metabolic switches (114,115), as well as an overall tissue context where aberrant interactions between resident cells lead to inflammation and fibro-adipogenesis (116–118). This has progressively led to a complex picture involving interdependent homeostatic perturbations and to date, the identification of prevalent pathological features driving the initiation of DMD is hardly feasible.

The skeletal myogenesis modelled here by the differentiation of hiPSCs, without gene overexpression or cell sorting, homogeneously and robustly recapitulates key developmental steps – pluripotency, mesoderm, somite and skeletal muscle – without any trace of other lineages. Therefore, it is a suitable dynamic model for studying human skeletal muscle development in both healthy and DMD cells, offering the possibility to clarify the consequences of the absence of dystrophin at each step of the differentiation process, as well as to explore dystrophin functions and find earlier and more specific disease biomarkers.

As previously observed with pluripotent stem cells (119), hiPSC-derived myotubes at day 25 displayed an embryonic/foetal gene expression profile. However, a clear distinction must be made between the nature of the expressed isoforms – embryonic / foetal / postnatal – and the degree of differentiation. For instance, hiPSC-derived myotubes expressed multiple markers of terminally differentiated muscles at levels higher than those measured in tissue-derived myotubes. With the idea of exploring human DMD phenotypes during

muscle development, we argued that generating embryonic/foetal myotubes from hiPSCs would not be a limitation.

In qualitative terms, DMD hiPSC-derived myotubes showed an overall morphology similar to healthy controls, with cell fusion and clear striation patterns, suggesting that the potential impact of dystrophin during *in vitro* differentiation is subtle and does not prevent myotube formation. However, our unbiased mRNA-seq analysis highlighted striking transcriptome dysregulations with 3,578 differentially expressed genes at day 25. This includes numerous genes which can be linked to previously described DMD phenotypes such as 1) DAPC dissociation (120); 2) rupture of calcium homeostasis (110); 3) myomiR downregulation (61,121); 4) sarcomere destabilisation (122–124); 5) mitochondrial and metabolism dysregulations (114,115); 6) NMJ fragmentation (125,126) and 7) fibrosis (118,127). It is interesting to note that these phenotypes are already detected at the transcriptional level in embryonic/foetal myotubes, while they usually appear postnatally in Human and other animal models. In addition, most of them are often considered as consequences of degeneration-regeneration cycles typical of DMD muscles *in vivo* (123,128,129) which are absent in our *in vitro* model, indicating that a part of these defects are primarily due to the absence of dystrophin itself. In particular, our data suggest that fibrosis is an intrinsic feature of DMD skeletal muscle cells, and therefore, it does not absolutely require a specific tissue context or additional cell populations to be detected *in vitro*. Fibrosis is a major hallmark of DMD pathophysiology, and the regulation of this process has been largely investigated in the past (107,130). A long-debated question is the implication of the TGFβ signalling pathway (131). In our model, TGFβ signalling was inhibited up to day 17 by inhibitors in the cell culture media, and TGFβ-related genes were not upregulated at day 25, suggesting that the observed fibrosis is TGFβ- independent.

Since several studies on Human and other animal models had described dystrophic phenotypes in DMD foetuses/infants (9–14), we investigated the precise timing of disease onset in our hiPSC-derived myotubes. First, the absence of dystrophin does not modify the capacity of cells derived from adult tissue biopsies to be reprogramed using the approach developed by Takeshi and Yamanaka (132). Both healthy and DMD cells retained pluripotency and the capacity to enter the mesoderm compartment at day 3. At that time, the embryonic dystrophin Dp412e is expressed and only marginal dysregulations are observed in DMD cells, *a priori* unrelated to cell fate choice as cells only express paraxial mesoderm markers at level similar to healthy controls.

DMD dysregulations are greatly increased at day 10, when cells express somite markers without any trace of transcripts coding for the long dystrophin isoform Dp427m expressed in skeletal muscles (only the ubiquitous variant Dp71-40 is found). At that time, we noticed few significant dysregulations of cell lineage markers, which became more prevalent at day 17 and 25. This might be an indication that to some extent, cell fate is misguided in DMD cells, where skeletal muscle markers are underexpressed and replaced by markers of alternative lineages, such as chondrocytes.

First visible at day 10, we identified mitochondrial dysregulation as one of the key processes happening in an orderly manner. Interestingly, early observations prior the discovery of the *DMD* gene had hypothesised that DMD was a mitochondrial/metabolic disease based on protein quantifications and enzyme activities (114,133). Later, mitochondria was identified as a key organelle in DMD, responsible for metabolic perturbations but also calcium accumulation and generation of reactive oxygen species (110–113). In this study, numerous genes coding for proteins located in the outer mitochondrial membrane start to be downregulated from day 10 in DMD cells, such as the benzodiazepine receptor TSPO, a member of the controversial mitochondrial permeability transition pore (mPTP) (109). The mPTP is a multiprotein complex whose members are not all precisely identified, and several studies suggest that it might be involved in DMD pathophysiology (134,135). A chicken-and-egg question currently debated relates to the initiation of these homeostatic breakdowns, as positive feedbacks exist between mitochondria, oxidative stress and calcium homeostasis dysregulations (111,112). In our model, dysregulations of genes controlling calcium homeostasis were detected after day 10, suggesting that mitochondrial impairment starts early and has predominant consequences in DMD, as hypothesised by Timpari *et al*. (108). Further experiments are needed to better evaluate the impact of mitochondrial dysregulations at the functional level.

Day 17 marks the entry in the skeletal muscle compartment with the expression of specific transcription factors, cell surface markers, the skeletal muscle variant of dystrophin (*Dp427m*), as well as myomiRs. It also marks the initiation of the skeletal muscle gene dysregulations observed at the myotube stage (*i.e.* downregulation of genes involved in DAPC and calcium homeostasis). For instance, the upregulation of fibrosis-related genes observed in DMD myotubes at day 25 is already visible at day 17, with the upregulation of the SHH pathway as well as collagen-related genes. In this study, it is seen as an early indicator of DMD physiopathology, confirming previous observations in DMD infants, both transcriptionally (4) and histologically (136,137).

Moreover, several myomiRs were found downregulated at days 17 and 25 and seem to play a central part in multiple DMD phenotypes. Besides their role in myogenesis (68,69), myomiRs can be involved in calcium homeostasis (138), metabolism and mitochondrial functions (139,140), and fibrosis (106,141). In particular, *MIR1-1* and *MIR206* are known to target key genes such as CACNA1C (138), CTGF (106), RRBP1 (141), several regulators of the pentose phosphate pathway (139), and even transcripts encoded by the mitochondrial genome (140). Even though the functional consequences of the multiple gene and myomiR dysregulations highlighted in this study is virtually impossible to anticipate, we believe that myomiRs can be key players in DMD biology.

Only few studies argued that DMD starts before the expression of the muscular dystrophin protein (18,142). Our data supports this idea as disease phenotypes seem to be initiated at the somite stage where Dp427m was not even transcribed. This could be explained by the deficit in other dystrophin isoforms expressed prior day 10, such as Dp412e at day 3 (15), but also by the decrease or loss of other RNA products expressed from the *DMD* locus, such as the ubiquitous isoform Dp71-40 or long non-coding RNAs (143). The lack of knowledge around these additional products contrasts with the extensive amount of data on the structure and function of the main muscular isoform Dp427m whose most studied role is to stabilise muscle cell membrane during contraction (144). Other tissue specific isoforms have been described, *e.g.* in the retina (Dp260 (30)) and in the brain (Dp427c (31), Dp427p (29) and Dp140 (28)), some of which are also slightly expressed in skeletal muscles under certain circumstances (145), but their role remains mostly unknown. Interestingly, in our data, the expression of Dp260 follows the same pattern of expression as Dp427m. It has been shown that the expression of Dp260 in *mdx*/utrnK/K mice can rescue the *mdx* phenotype (146), indicating overlapping functions between Dp427m and Dp260. On the other hand, it is now well established that a third of DMD patients display cognitive deficiencies – which might be correlated with mutations affecting Dp140 (147) – attesting that dystrophin can be involved in other cell functions.

To date, the standard of care for DMD patients helps mitigate and delay some of the most severe symptoms but remains insufficient to have a curative effect. Despite decades of work with the *mdx* mouse model, only a few pharmacological candidate molecules have moved forward to clinical trials, with variable efficiency. As several gene therapy trials have been recently initiated with promising preliminary data, we believe that our human *in vitro* model system might be useful for the development of combination therapies. Recent studies

have proved that the association of two different therapeutic approaches could have a synergistic effect on the overall treatment outcome, and can be used for instance to boost the effect of dystrophin re-expression by antisense oligonucleotides or gene therapy (8,148,149). Here, our extensive RNA-seq data could help identify relevant therapeutic targets for pharmacological intervention, such as CTGF – involved in fibrosis and found upregulated in DMD myotubes – which can be inhibited by monoclonal antibodies (150), or TSPO receptor – a receptor potentially member of the mPTP downregulated in DMD cells – targetable with benzodiazepines (151). In addition, our model might also be used as a platform to screen pharmacological compounds in an unbiased high-throughput manner. Indeed, skeletal muscle progenitor cells at day 17 can be robustly amplified, cryopreserved and plated in a 384-well plate format (data not shown). Thus, they could be an interesting tool to highlight pharmacological compounds to be used alone, or in combination with gene therapy.

To summarise, the directed differentiation of hiPSCs without gene overexpression or cell sorting homogeneously and robustly recapitulates key developmental steps of skeletal myogenesis and generates embryonic/foetal myotubes without any trace of other lineages. The absence of dystrophin does not compromise cell reprogramming, pluripotency or the entry into the mesoderm compartment. While none of the long dystrophin isoform is expressed, a significant transcriptome dysregulation can be observed at the somite stage that implicates mitochondria prior to defects in calcium homeostasis. Although being able to enter the skeletal lineage compartment and become myotubes, DMD cells exhibit an imbalance in cell fate choice as they express lower amount of key muscle proteins and retain basal expressions of other lineages, leading to the well-characterised DMD phenotypes including muscle features and metabolism dysregulations as well as fibrosis. Altogether, these data argue for 1) a deficit and not a delay in DMD differentiation; 2) seeing DMD as a progressive developmental disease as well as a metabolic pathology whose onset is triggered before the entry into the skeletal muscle compartment; and 3) fibrosis as an intrinsic feature of DMD muscle cells. Future studies could explore the additional roles of *DMD* locus products with the impact of their loss all along the skeletal muscle development, as well as find earlier and more specific disease biomarkers and develop combination therapeutic strategies using high-throughput drug screening.

Materials and methods

Ethics, consent, and permissions

At the Cochin Hospital-Cochin Institute, the collection of primary cultures of myoblasts was established from patient muscle biopsies conducted as part of medical diagnostic procedure of neuromuscular disorders. For each patient included in this study, signed informed consent was obtained to collect and study biological resources, and establish primary cultures of fibroblasts and myoblasts at the Hospital Cell Bank-Cochin Assistance Publique—Hôpitaux de Paris (APHP). This collection of myoblasts was declared to legal and ethical authorities at the Ministry of Research (number of declaration, 701, n° of the modified declaration, 701–1) via the medical hosting institution, APHP, and to the "Commission Nationale de l'Informatique et des Libertés" (CNIL, number of declaration, 1154515).

Cells

Human primary adult myoblasts from healthy individuals and DMD patients were provided by Celogos and Cochin Hospital-Cochin Institute (Table S3). In Celogos laboratory, cell preparation was done according to patent US2010/018873 A1.

Cell culture

Human tissue-derived myoblasts – Primary myoblasts were maintained in a myoblast medium: DMEM/F-12, HEPES (31330–038, Thermo Fisher Scientific) supplemented with 10 % fetal bovine serum (FBS, Hyclone, Logan, UT), 10 ng/mL fibroblast growth factor 2 (FGF2, 100-18B, Peprotech), and 50 nM Dexamethasone (D4902, Sigma-Aldrich) on 0.1 % gelatin (G1393, Sigma-Aldrich) coated culture ware.

Human tissue-derived myotubes – Primary myoblasts were differentiated into myotubes. Cells were seeded at 600 cells/cm^2 on 0.1 % gelatin coated cultureware in myoblast medium containing 1 mM Acid ascorbic 2P (A8960, Sigma-Aldrich).

Human induced pluripotent stem cells – Primary myoblasts were reprogrammed into hiPSCs following the protocol described in (15), using the Yamanaka's factors POU5F1, SOX2 and KLF4 transduction by ecotropic or amphotropic vectors (Table S3). HiPSCs were adapted and maintained with mTeSR™1 culture medium (05850,

Stemcell Technologies) on Corning® Matrigel® Basement Membrane Matrix, lactose dehydrogenase elevating virus (LDEV)-Free-coated cultureware (354234, Corning Incorporated). Cells were then seeded at 20,000 cells/cm^2, passaged and thawed each time with 10 µM StemMACS™ Y27632.

Human iPSC-derived cell – Six hiPSCs (3 healthy and 3 DMD) were differentiated three times toward skeletal muscle lineage using commercial media designed from Caron's work (23) (Skeletal Muscle Induction medium SKM01, Myoblast Cell Culture Medium SKM02, Myotube Cell Culture Medium SKM03, AMSbio). This protocol is a 2D directed differentiation that uses 3 consecutive defined media (SKM01 from day 0 to 10, SKM02 from day 10 to 17 and SKM03 from day 17 to d25) and only one cell passage at day 10. Cells were seeded at 3,500 cells/cm^2 at day 0 and day 10 on BioCoat™ Collagen I cultureware (356485, Corning Incorporated). Part of the cell culture was frozen at day 17 for further experiments such as DNA extraction. These cells were then thaw at 30,000 cells/cm^2, and cultured in SKM02 for 3 days and SKM03 for 3 additional days to get myotubes.

DNA and RNA experiments

RNA extraction and quality – RNA extraction was done in the six cell lines at 7 different time points: tissue-derived myoblast and tissue-derived myotube, as well as during hiPSC differentiation at day 0, 3, 10, 17 and 25 (hiPSC-derived myotube) using the miRNeasy Mini kit (217004, QIAgen) on the QIAcube instrument. RNAs coming from the part A of the extraction protocol was used for mRNA-seq and RT-qPCR. RNAs coming from the part B of the extraction protocol was used for miRseq. PartA RNA was quantified on Nanodrop spectrophotometer (ND-1000, Thermo Fisher Scientific) and purity/quality (RIN ≥ 7) was assessed on the 2200 TapeStation using the Agilent RNA ScreenTape (5067-5576 / 5067-5577 / 5067-5578, Agilent). PartB RNA was quantified and purity/quality was assessed on the 2100 Agilent BioAnlayzer using the Agilent small RNA kit (5067-1548, Agilent).

Reverse transcription – 500 ng of total RNA were reverse transcribed with random primers (48190–011, Thermo Fisher Scientific), oligo(dT) (SO131, Thermo Fisher Scientific), and deoxynucleotide (dNTP, 10297–018, Thermo Fisher Scientific) using Superscript® III reverse transcriptase (18080–044, Thermo Fisher Scientific). Thermocycling conditions were 10 min, 25 °C; 60 min, 55 °C; and 15 min, 75 °C.

qPCR **–** We amplified cDNA/total DNA using primers (Thermo Fisher Scientific) listed in Table S4. They were designed using Primer blast (http://www.ncbi.nlm.nih.gov/tools/primer-blast). The amplification efficiency of each primer set was preliminarily determined by running a standard curve. Detection was performed using a QuantStudio™ 12K Flex Real-Time PCR System (Thermo Fisher Scientific). Reactions were carried out in a 384-well plate, with 10 µL containing 2.5 µL of 1/10 cDNA or 6.25 ng/uL total DNA, 0.2 µL of mixed forward and reverse primers at 10 µM each, and 5 µL of 2X Luminaris Color HiGreen qPCR Master Mix Low Rox (K0973, Thermo Fisher Scientific). Thermocycling conditions were 50 °C during 2 min, 95 °C during 10 min, followed by 45 cycles including 15 sec at 95 °C, 1 min at 60 °C plus a dissociation stage. All samples were measured in triplicate. Experiments were normalised using UBC as reference gene and relative quantification was done with the ΔΔCt method.

mRNA-seq **–** Libraries are prepared with TruSeq Stranded mRNA kit protocol according supplier recommendations. Briefly, the key stages of this protocol are successively, the purification of PolyA containing mRNA molecules using poly-T oligo attached magnetic beads from 1µg total RNA, a fragmentation using divalent cations under elevated temperature to obtain approximately 300bp pieces, double strand cDNA synthesis and finally Illumina adapter ligation and cDNA library amplification by PCR for sequencing. Sequencing is then carried out on paired-end 100 b/75 b of Illumina HiSeq 4000.

An RNA-seq analysis workflow was designed using snakemake 3.5.4 (152) for read quality estimation, mapping and differential expression analysis. Quality estimation was obtained with FastQC 0.11.5 (https://www.bioinformatics.babraham.ac.uk/projects/fastqc/). Mapping to the human genome assembly Ensembl GRCh37.87 (43,695 transcripts) was performed with STAR 2.5.0a (153). According to STAR manual and for more sensitive novel junction discovery, the junctions detected in a first round of mapping were used in a second mapping round. Read strandness was confirmed using RSeQC (154). Expression counts at the gene level were calculated using FeatureCounts 1.4.6 (155). Analysis results were summarised using MultiQC 1.0 (156). Normalised counts (median ratio normalisation, MRN) and differential expression analysis was performed with DESeq2 1.16.1 (157), considering pairwise comparisons with all developmental stages and comparing DMD versus healthy cells within developmental stages. BiomaRt 2.30.0 (158) was used to fetch gene annotations from Ensembl. Transcripts with $|\log2FoldChange| \geq 0.4$ (equivalent of DMD/healthy ratio ≤ 0.76 or ≥ 1.32) and adjusted pvalue ≤ 0.05 were considered differentially expressed. RNA-seq data have been

deposited in the ArrayExpress database (159) at EMBL-EBI under accession number E-MTAB-8321 (https://www.ebi.ac.uk/arrayexpress/experiments/E-MTAB-8321).

miRNA-seq **–** 10 ng of miRNA was reverse transcribed using the Ion Total RNA-seq kit v2 (4475936, Thermofisher Scientific) following the protocol of the manufacturer for small RNA libraries. The cDNA libraries were amplified and barcoded using Ion Total RNA-seq kit v2 and Ion Xpress RNA-seq Barcode Adapters 1-16 Kit (Thermofisher Scientific). The amplicons were quantified using Agilent High Sensitivity DNA kit before the samples were pooled in sets of fifteen. Emulsion PCR and enrichment was performed on the Ion OT2 system Instrument using the Ion PI Hi-Q OT2 200 kit (A26434, Thermofisher Scientific). Samples were loaded on an Ion PI v3 Chip and sequenced on the Ion Proton System using Ion PI Hi-Q sequencing 200 kit chemistry (200 bp read length; A26433, Thermofisher Scientific). Sequencing reads were trimmed with Prinseq (160) (v0.20.4) (--trim-right 20) and filtered by average quality score (--trim-qual 20). Reads with a size less than 15 bp have been removed and reads with a size greater than 100 bp have been trimmed with Cutadapt (v1.16)(161). Mapping to the human genome assembly Ensembl GRCh37.87 (3111 transcripts) was performed with STAR 2.5.3a (153)**.** Normalised counts (median ratio normalisation, MRN) and differential expression analysis was performed with DESeq2 1.16.1 (157), considering pairwise comparisons with all developmental stages and comparing DMD versus healthy cells within developmental stages. Transcripts with $|\log2FoldChange| \geq 0.4$ (equivalent of DMD/healthy ratio ≤ 0.76 or ≥ 1.32) and pvalue ≤ 0.05 were considered differentially expressed. The use of pvalue instead of adjusted pvalue is justified by biological meaning(162) (i.e. well-known regulated / dysregulated miRNAs had a pvalue ≤ 0.05 but not an adjusted pvalue ≤ 0.05). miRNA-seq data have been deposited in the ArrayExpress database (159) at EMBL-EBI under accession number E-MTAB-8293 (https://www.ebi.ac.uk/arrayexpress/experiments/E-MTAB-8293).

High-throughput data analyses **–** Graphs were realised using RStudio. Viridis library (163) was used for the colour palette easier to read with colour blindness and print well in grey scale. For unsupervised analyses, normalised counts were standardised with scale function (center = TRUE, scale = TRUE) and plotted with corrplot function from corrplot library (164). Spearman correlation was done with the cor function (method = "spearman", use = "pairwise.complete.obs") on standardised data. Hierarchical clustering and heatmap were performed with gplots library (165) heatmap.2 function on standardised data. Gene enrichment data were retrieved from DAVID database using RDAVIDWebService library (166) on supervised list of mRNAs (mRNA-seq

499 data: adjusted pvalue ≤ 0.01, normalised counts ≥ 5 in at least one sample, ratio ≤ 0.5 or ≥ 2 for myogenesis
500 (Figure S2B) and ratio ≤ 0.76 or ≥ 1.32 for DMD phenotype (Figure S2C); enrichment data: Benjamini value ≤
501 0.05, enrichment ≥ 1.5). Only Gene Ontology terms were processed.

502 **Protein experiments**

503 ***Immunolabelling*** **–** Cells (healthy hiPSC 1/ DMD hiPSC 2, Table S3) at day 17 of culture were thawed and
504 seeded at 10,000 cells/cm^2 in SKM02 medium in Falcon® 96-well microplate (353219, Corning) coated with
505 0.1% gelatin (G1393, Sigma-Aldrich) and 2.4 µg/mL laminin (23017015, Thermofischer Scientific) in PBS 1X
506 (D8537, Sigma-Aldrich). After 4 days, cells were switched to DMEM/F-12, HEPES (31330038, Thermofischer
507 Scientific) with 2% Horse serum (H1270, Sigma-Aldrich). Before staining, after removing the culture medium,
508 cells were fixed 15 min at 4°C with PFA 4% (15710, Euromedex) after 7 days of culture. A first quick Phosphate
509 buffered saline (PBS) 1X tablets (P4417, Sigma-Aldrich) wash was done, followed by another lasting 10 min.
510 Then, a solution with PBS 1X, Triton™ X-100 0.25% (T8787, Sigma-Aldrich) and Bovine serum albumin 2.5%
511 (BSA, A9418, Sigma-Aldrich) was added and incubated 30 min at room temperature. Primary antibody was
512 finally added, diluted in the same buffer (α-actinin 1/500, A7811, Sigma-Aldrich), overnight at 4°C. The next
513 day, two quick PBS 1X washes were followed by a third incubated 10 min at room temperature. An incubation
514 was done 45 min at room temperature with a mix of 4',6-Diamidine-2'-phenylindole dihydrochloride (DAPI,
515 1µg/mL, 10236276001, Sigma-Aldrich) and the secondary antibody Donkey anti-Mouse Alexa Fluor 555 in PBS
516 1X, (1/1000, A-31570, Thermofischer Scientific). Finally, two quick PBS 1X washes were followed by a third
517 incubated 10 min at room temperature. The stained cells were kept in PBS 1X at 4°C before imaging with a
518 Zeiss LSM880 Airyscan confocal and Zen software (Black edition).

519 ***Western blotting*** **–** For tissue-derived myotubes, after three rinses with cold PBS 1X (w/o Ca2+ and Mg2+,
520 D8537, Sigma-Aldrich), protein extracts were isolated from cultured cells by scraping (010154, Dutscher) with
521 an extraction protein buffer (NaCl 150 mM, Tris 50 mM, EDTA 10 mM (AM9260G, ThermoFisher Scientific),
522 Triton 1X, 1/100 Protease Inhibitor Cocktail (P8340, Sigma-Aldrich), PhosSTOP tablet (04906845001, Roche
523 Diagnostics)). For hiPSC-derived myotubes, cell pellets were rinsed once with cold PBS 1X, spun 5 min at 300 g
524 and resuspended in the same extraction protein buffer. Protein Extracts were centrifuged at 4°C 10 min at
525 16,000 g and supernatants were kept at −80 °C. Quantitation of total protein was done with Pierce BCA protein

assay kit (23225, ThermoFischer Scientific). Before gel loading, protein extracts were mixed with 9µL of loading buffer (Urea 4M, SDS 3.8%, Glycerol 20%, Tris 75mM pH 6.8, 5% β-mercaptoethanol, 0.1mg/mL Bromophenol blue) and completed to 28µL (for one well) with extraction protein buffer, then heated once 5 min at 95 °C. Western blots were performed either with Criterion ™ XT Tris-Acetate Precast Gels 3–8 % (3450130, Bio-Rad, Hercules, CA), XT Tricine running buffer (161–0790, Bio-Rad) and ran at room temperature for 1 hour and 15 min at 150 V for RYR1 (1/1000, MA3-925, ThermoFisher Scientific), MF20 (1/500, DSHB, concentrate), Manex50 (1/30, DSHB), α-sarcoglycane (1/150, A-SARC-L-CE, Leica biosystems), γ-sarcoglycane (1/150, G-SARC-CE, Leica biosystems), or with 4–15% Criterion™ TGX™ Precast Midi Protein Gel (5671084, Bio-Rad), 10x Tris/Glycine/SDS Running Buffer (1610772), and ran at room temperature for 1 hour at 200 V for CaV1.1 (1/1000, MA3-920, ThermoFisher Scientific), ATP5A (1/1,000, ab14748, ABCAM), Semaphorin 6A (1/55, AF1146, R&D systems) and GLI3 (1/200, AF3690, R&D systems). Gels were rinsed once in water and blotted either with “high molecular weight” or “mixed molecular weight” program of TransBlot® Turbo™ transfer system (Bio-Rad) using Trans-Blot®Turbo™ Midi Nitrocellulose Transfer Packs (170–4159, Bio-Rad). Blots were then processed with the SNAP i.d.® 2.0 Protein Detection System following the manufacturer’s protocol, with Odyssey® Blocking Buffer (927-40003, LI-COR) for blocking and with 0,2% Tween® 20 added for antibody dilutions (28829.296, VWR), washes were done with phosphate-buffered saline tween (PBST) buffer (PBS 1X tablets, P4417, Sigma-Aldrich; 0.1 % Tween® 20). Every primary antibody was pooled with either α-actinin (1/12,500, sc-17829, Santa Cruz or 1/7000, A7811, Sigma-Aldrich) or α-tubulin (1/6666, Ab7291, Abcam). For secondary antibodies, either IRDye 800CW donkey anti-mouse and/or IRDye® 680RD donkey anti-goat were used (1/5000-1/10000, 926-32212, 926-68074, LI-COR). After completion of SNAP i.d.® general protocol, with the membrane still in the blot holder, two PBS 1X washes were finally done before band visualisations with Odyssey® CLx Imaging System and quantification with Image Studio Lite software (Version 5.2). Statistical analysis was performed using unpaired t test on GraphPad Prism software.

TMT Isobaric quantitative proteomics –

Samples Preparation: Cells at day 17 were collected and resuspended in 90% FBS (Hyclone), 10% DMSO (A3672.0050, VWR), cooled down until -90°C with the CryoMed™ device (ThermoFisher Scientific), before storage in liquid nitrogen. Cells were then thawed and washed 5 times with cold PBS and air was replaced by Argon to thoroughly dry the pellet that was flash frozen in liquid nitrogen. 5-10 times the approximate cell

554 pellet volume of 0.5 M triethyl ammonium bicarbonate (TEAB) with 0.05% SDS was added to the cell pellet for
555 protein extraction. Cell pellet was re-suspended and triturated by passing through a 23-gauge needle and 1ml
556 syringe for 30 times. Samples were then sonicated on ice at amplitude of 20% for 30 x 2 sec bursts and
557 centrifuged at 16000g for 10 min at 4°C. Supernatant was transferred to a fresh Eppendorf tube. Protein was
558 quantified by nanodrop. 100-150µg of protein was aliquoted for each individual sample and 2µl TCEP (50mM
559 tris-2-carboxymethyl phosphine) was added for every 20µl of protein used for reducing the samples. After 1 hr
560 incubation at 60°C, 1µl MMTS (200mM methylmethane thiosulphonate) was added for every 20µl of protein
561 used for alkylating/'blocking' the samples. Finally, after a 10 min incubation at RT, samples were trypsinised by
562 addition of 6-7.5µl of 500ng/µl trypsin. The ration between enzyme: substrate was 1:40. Samples were
563 incubated overnight at 37°C in the dark. *TMT labelling:* When TMT reagents reached room temperature, 50µl
564 of isopropanol/[acetonitrile] was added to each TMT 11-plex reagent and was incubated at RT for 2 hrs, in the
565 dark. 8 µl of 5% hydroxylamine was added to neutralise the reaction. Each sample was separately lyophilised
566 at 45^{o}C. Samples have been stored at -20^{o}C or used immediately.
567 *Offline C4 High Performance Liquid Chromatography (HPLC):* All 8 samples were pooled together in 60µl of 97%
568 mobile phase A (99.92% % H2O, 0.08% NH_4OH) and 3% mobile phase B (99.92% % Acetonitrile, 0.02% NH_4OH)
569 by serially reconstituting each sample. Extra 40µl of mobile phase was added to sample 1, after sample has
570 been well vortexed, all the contents of sample 1 tube were transferred to the tube with the sample 2 (and
571 serially repeated until all samples were pooled). Final volume of samples needed to be 100µl. After sample was
572 centrifuged at 13000g for 10 min, supernatant was collected with an HPLC injection syringe. 100µl was injected
573 onto the sample loop. Fractions were collected in a peak dependent manner. Finally, fractions were lyophilised
574 at 45^{o}C and stored at -20^{o}C until required. The used column was a Kromasil C4 column 100Å pore size, 3.5µm
575 particle size, 2.1mm inner diameter and 150mm length. The gradient for C4 separation was (RT in min - %B): 0-
576 3; 10-3; 11-5; 16-5; 65-20; 100-30; 15-80; 120-80; 125-3.
577 *Solid Phase Extraction Cleaning of peptides fractions:* A GracePureTMT SPE C18-Aq cartridge was used for pre-
578 cleaning of samples (Support: Silica, % Carbon: 12.5%, With endcapping, Surface area: 518m^2/g, Particle size:
579 50µm, Pore size: 60Å, Water-wettable). Samples were reconstituted using in total 400µl of 1% ACN, 0.01% FA.
580 Cartridge was washed with 600µl of ACN. ACN was then completely flushed out of the column at dropwise
581 speed. This activated the ligands. Then 1% ACN, 0.01% FA (600µl) was flushed through the cartridge to
582 equilibrate the sorbent. 400µl of the sample was loaded in the cartridge. It was then very slowly flushed

583 through the cartridge and recovered into a fresh tube. This process was repeated 3 times. 2 volumes of 250µl
584 of 1%ACN, 0.01%FA were used to clean and de-salt the sample. It was flushed through very slowly. 2 volumes
585 (250µl each) were used per step (2% ACN, 10% ACN, 30% ACN, 50% ACN, 70% ACN). This cycle was repeated
586 twice. Each particular concentration was pooled in one tube. Samples were dried to dryness in a Speedvac at
587 RT overnight and stored at -20^{o}C. Like previously, samples were pooled with 100µl of 97% mobile phase A
588 (99.92% % H2O, 0.08% NH_4OH) and 3% mobile phase B (99.92% % Acetonitrile, 0.02% NH_4OH) and injected
589 onto the sample loop. Fractions were collected in a peak dependent manner. The gradient for SPE cleaned
590 peptides C4 separation (RT in min - %B): 0-2; 10-2; 20-5; 25-5; 35-20; 55-35; 60-35; 70-80; 75-80; 80-3.
591 *Online C18 High Precision Liquid Chromatography (HPLC):* 30µl of loading phase (2% acetonitrile, 1.0% formic
592 acid) was added to each fraction-containing Eppendorf tube. Samples were vortexed and centrifuged. Blanks
593 (30µl mobile phase) were added into well A1 to A12. 30µl of sample 1 was pipetted into well B1, sample 2 in
594 well B2 and so on. An orthogonal 2D-LC-MS/MS analysis was performed with the Dionex Ultimate 3000 UHPLC
595 system coupled with the ultra-high-resolution nano ESI LTQ-Velos Pro Orbitrap Elite mass spectrometer
596 (Thermo Scientific).
597 *Data analysis:* HCD and CID tandem mass spectra were collected and submitted to Sequest search engine
598 implemented on the Proteome Discoverer software version 1.4 for peptide and protein identifications. All
599 spectra were searched against the UniProtKB SwissProt. The level of confidence for peptide identifications was
600 estimated using the Percolator node with decoy database searching. False discovery rate (FDR) was set to 0.05,
601 and validation was based on the q-Value. Protein ratios were normalised to protein median and peptides with
602 missing TMT values were rejected from protein quantification. Phosphorylation localisation probability was
603 estimated with the phosphoRS node. Protein ratios were transformed to $\log_2$ ratios and significant changes
604 were determined by one sample T-test. To reduce the impact of possible false positive identifications, more
605 parameters were set: 1) only proteins with more than two quantified unique peptides. 2) DMD/Healthy ratio ≥
606 1.32 or ≤ 0.76 and 3) only FDR corrected pvalue ≤ 0.05 were retained for bioinformatics analysis. The list of
607 proteins quantified in the 6 samples is in Table S5. Proteomic data have been deposited in the PRIDE Archive
608 database (167) at EMBL-EBI under accession number PXD015355
609 (https://www.ebi.ac.uk/pride/archive/projects/PXD015355).

Competing interests

The authors declare that they have no competing interests.

Funding

We thank the Fondation Maladies Rares (GenOmics grant), Labex Revive (Investissement d'Avenir; ANR-10-LABX-73) and the AFM Téléthon for funding this project.

Acknowledgements

The RNA-Sequencing libraries were processed and sequenced by Integragen (Evry, France). We gratefully acknowledge support from the PSMN (Pôle Scientifique de Modélisation Numérique) of the ENS de Lyon for the computing resources. We thank Dr Nacira Tabti, Dr Elisabeth Le Rumeur, Dr Nathalie Deburgrave and Dr Malgorzata Rak for providing us with specific reagents and antibodies. We thank Dr David Israeli for his feedback on the manuscript and overall discussion on our project.

Figure legends

Figure 1 – Differentiation dynamics of hiPSCs (D0) into MyoT (D25) in healthy cells at the transcriptomic level. A) Spearman correlation matrix of transcriptomes (mRNAs, right) and miRnomes (miRNAs, left). Yellow dots indicate a stronger correlation. **B)** Heatmap of selected differentiation markers. (D: day; hiPSC: human induced pluripotent stem cell; MyoT: myotube).

Figure 2 – Differentiation dynamics of hiPSCs (D0) into MyoT (D25) in DMD cells. A) Dotplot of DMD/healthy expression ratios of selected markers. Statistical differences are indicated in brackets after gene names, and grey circles around the corresponding dots. **B)** Proportions of significantly dysregulated mRNAs (adjusted pvalue ≤ 0.05) in DMD cells at each time points. Expression of **C)** *MIR1-1* and **D)** *ATP2A2* mRNA during differentiation, as well as **E)** ATP2A2 protein level at D17. (*adjusted pvalue ≤ 0.05, **adjusted pvalue ≤ 0.01, ***adjusted pvalue ≤ 0.001, ****adjusted pvalue ≤ 0.0001; D: day; hiPSC: human induced pluripotent stem cell; MyoT: myotube).

Figure 3 – Comparison of healthy and DMD MyoT from hiPSCs and tissues at the protein level. A) hiPSC-derived MyoT immunolabelling of α-actinin (red) and nuclei (DAPI, blue) in healthy (left) and DMD cells (right). **B)** Representative Western blots and related quantifications of DMD, SGCA, SGCG, myosin heavy chains, CACNA1S and RYR1 from protein extracts in healthy and DMD hiPSC-derived and tissue-derived MyoT (X: 0.25 µg of total protein was used in hiPSC-derived MyoT instead of 7µg in tissue-derived MyoT - *pvalue ≤ 0.05, **pvalue ≤ 0.01, ***pvalue ≤ 0.001, ****pvalue ≤ 0.0001). (hiPSC: human induced pluripotent stem cell; MyoT: myotube).

Figure 4 – Manifestation of the DMD phenotype in the transcriptomes and miRnomes of myotubes derived from hiPSCs and tissues. A) Hierarchical clustering and heatmap in healthy hiPSCs (D0), hiPSC-derived MyoT and tissue-derived MyoT with selected skeletal muscle transcripts and miRNAs. **B)** Volcano plots of dysregulated mRNAs/miRNAs in hiPSC-derived MyoT (left) and tissue-derived MyoT (right) – vertical grey dashed lines represent DMD/Healthy ratio thresholds at 0.76 or 1.32 - the horizontal grey dashed line represents the adjusted pvalue threshold at 0.05. (DAPC: dystrophin-associated protein complex; hiPSC: human induced pluripotent stem cell; MyoT: myotube; NMJ: neuromuscular junction; TF: transcription factor).

Figure 5 – Illustration of the fibrosis phenotypes in DMD cells. Volcano plots of dysregulated mRNAs/miRNAs related to **A)** the SHH pathway and collagen metabolism at D10/17/25; and **B)** fibrosis at D25 – vertical grey dashed lines represent DMD/Healthy ratio thresholds at 0.76 or 1.32 - the horizontal grey dashed line represents the adjusted pvalue threshold at 0.05. (D: day; MMP: matrix metallopeptidase; SHH: sonic hedgehog pathway; TIMP: tissue inhibitor of metallopeptidase; TGF: transforming growth factor).

Figure 6 – Illustration of the metabolic and mitochondrial phenotypes in DMD cells. Volcano plots of dysregulated mRNAs/miRNAs related to **A)** principal metabolic pathways; and **B)** the constitution of the five mitochondrial respiratory complexes in DMD hiPSC-derived MyoT – vertical grey dashed lines represent DMD/Healthy ratio thresholds at 0.76 or 1.32 - the horizontal grey dashed line represents the adjusted pvalue threshold at 0.05. Quantification of ATP5A1 expression **C)** at the mRNA level during differentiation, and **D)** at the protein level at D17 (TMT proteomic data, left) and D25 (Western blot data, right). (*adjusted pvalue ≤ 0.05, **adjusted pvalue ≤ 0.01, ***adjusted pvalue ≤ 0.001, ****adjusted pvalue ≤ 0.0001). (D: day; hiPSC: human induced pluripotent stem cell, MyoT: myotube)

Figure 7 – Mitochondrial dysregulations in DMD cells during differentiation. A) Absolute (top) and relative numbers (%, bottom) of dysregulated genes from the different mitochondrial compartments over the course of DMD hiPSC differentiation. **B)** Expression ratios of selected mitochondrial proteins. Statistical differences are indicated in brackets (*adjusted pvalue ≤ 0.05, **adjusted pvalue ≤ 0.01, ***adjusted pvalue ≤ 0.001, ****adjusted pvalue ≤ 0.0001). **C)** Volcano plots of mitochondria-related genes over the course of DMD hiPSC differentiation. Statistical differences are symbolised with orange dots – vertical grey dashed lines represent DMD/Healthy ratio thresholds at 0.76 or 1.32 - the horizontal grey dashed line represents the adjusted pvalue threshold at 0.05 – The percentage of significantly dysregulated genes is indicated at the bottom right in grey. (D: day).

Figure S1 – DMD variant expression over the course of hiPSC differentiation. A) Bright field microscope pictures at the 7 differentiation points giving rise to hiPSC-derived and tissue-derived MyoT. Possible cryopreservation time points are indicated by snowflakes. **B)** RT-qPCR relative quantification of *DMD* variants expression during differentiation of hiPSCs (D0) into MyoT (D25) with the related cycle threshold (CT) values (Ct: cycle threshold; D: day; hiPSC: human induced pluripotent stem cell; MyoB: myoblast; MyoT: myotube).

Figure S2 – Gene ontology enrichments over the course of healthy and DMD hiPSC differentiation A) Proportions of significantly regulated mRNAs (adjusted pvalue ≤ 0.01) between successive differentiation time points during the differentiation of healthy hiPSCs. Gene ontology enrichments on **B)** significantly regulated mRNAs between successive differentiation time points in healthy cells (number of genes in brackets) and **C)** significantly dysregulated mRNAs at each differentiation time points in DMD cells. The number of genes involved in these significant enrichments is indicated in brackets next to each GO term. In green, GO terms related to downregulated genes and in yellow, GO terms related to upregulated genes (BP: biological process; CC: cellular component; D: day; hiPSC: human induced pluripotent stem cell; MyoB: myoblast; MyoT: myotube).

Figure S3 – Comparison of healthy and DMD cells at D10 and D17, protein analyses. Western blots and quantifications of **A)** SEMA6A at D10, **B)** GLI3 at D10 and **C)** GLI3 at D17. (*pvalue ≤ 0.05, **pvalue ≤ 0.01, ***pvalue ≤ 0.001, ****pvalue ≤ 0.0001; D: day; GLI3FL: GLI3 full length; GLI3R: GLI3 repressor).

Figure S4 – Comparison of hiPSC-derived and tissue-derived MyoT for the expression of cell cycle genes and myogenic regulators. Hierarchical clustering and heatmap of **A)** selected cell cycle transcripts and miRNAs, and **B)** DLK1, IGF2 and selected myosin transcripts in hiPSCs (D0), hiPSC- and tissue-derived MyoT. **C)** Dotplot of DMD/healthy expression ratio of muscle transcription factors. Significant statistical differences are shown in brackets (*adjusted pvalue ≤ 0.05, **adjusted pvalue ≤ 0.01, ***adjusted pvalue ≤ 0.001, ****adjusted pvalue ≤ 0.0001). (hiPSC: human induced pluripotent stem cell; MyoT: myotube).

Figure S5 – Dysregulations of metabolic pathways and mitochondrial genes during differentiation of DMD hiPSCs. A) Scheme of metabolism dysregulations at day 25. Dotplots of **B)** mitochondrial transcripts, **C)** transcripts coding mitochondrial protein import, and **D)** transcripts coding mitochondrial transcription/replication; **E)** Mitochondrial DNA quantification by qPCR at D25. Dotplots of mitochondrial proteins expressed at D17 involved in **F)** protein import, **G)** mitochondrial transcription/replication. Statistics are in brackets (*adjusted pvalue ≤ 0.05, **adjusted pvalue ≤ 0.01, ***adjusted pvalue ≤ 0.001, ****adjusted pvalue ≤ 0.0001; D: day).

References

1. Hoffman EP, Brown RH, Kunkel LM. Dystrophin: the protein product of the Duchenne muscular dystrophy locus. Cell. 1987;51(6):919–28.

2. Koeks Z, Bladen CL, Salgado D, van Zwet E, Pogoryelova O, McMacken G, et al. Clinical Outcomes in Duchenne Muscular Dystrophy: A Study of 5345 Patients from the TREAT-NMD DMD Global Database. J Neuromuscul Dis [Internet]. 2017;4(4):293–306. Available from: http://www.ncbi.nlm.nih.gov/pubmed/29125504%0Ahttp://www.pubmedcentral.nih.gov/articlerender.fcgi?artid=PMC5701764

3. Liu M, Chino N, Ishihara T. Muscle damage progression in Duchenne muscular dystrophy evaluated by a new quantitative computed tomography method. Arch Phys Med Rehab. 1993;74(5):507–14.

4. Pescatori M, Broccolini A, Minetti C, Bertini E, Bruno C, D'amico A, et al. Gene expression profiling in the early phases of {DMD:} a constant molecular signature characterizes {DMD} muscle from early postnatal life throughout disease progression. {FASEB} J. 2007;21(4):1210–26.

5. Szigyarto C, Spitali P. Biomarkers of Duchenne muscular dystrophy: current findings. Degener Neurol Neuromuscul Dis. 2018;8:1–13.

6. Moat SJ, Bradley DM, Salmon R, Clarke A, Hartley L. Newborn bloodspot screening for Duchenne muscular dystrophy: 21 years experience in Wales {(UK).}. Eur J Hum Genet. 2013;21(10):1049–53.

7. Crone M, Mah JK. Current and Emerging Therapies for Duchenne Muscular Dystrophy. Curr Treat Options Neurol. 2018;20(8):31.

8. Ngoc L-N, Malerba A, Popplewell L, Schnell F, Hanson G, Dickson G. Systemic Antisense Therapeutics for Dystrophin and Myostatin Exon Splice Modulation Improve Muscle Pathology of Adult mdx Mice. Mol Ther - Nucleic Acids. 2017;6:15–28.

9. Nguyen F, Cherel Y, Guigand L, I G-L, Wyers M. Muscle lesions associated with dystrophin deficiency in neonatal golden retriever puppies. J Comp Pathol. 2002;126(2–3):100–8.

10. Bassett DI. Dystrophin is required for the formation of stable muscle attachments in the zebrafish embryo. Development. 2003;130(23):5851–60.

11. Merrick D, Stadler LK, Larner D, Smith J. Muscular dystrophy begins early in embryonic development deriving from stem cell loss and disrupted skeletal muscle formation. Dis Model Mech. 2009;2(7–8):374–88.

12. Emery AE. Muscle histology and creatine kinase levels in the foetus in Duchenne muscular dystrophy. Nature. 1977;266(5601):472–3.

13. Toop J, Emery AE. Muscle histology in fetuses at risk for Duchenne muscular dystrophy. Clin Genet. 1974;5(3):230–3.

14. Vassilopoulos D, Emery AE. Muscle nuclear changes in fetuses at risk for Duchenne muscular dystrophy. J Med Genet. 1977;14(1):13–5.

15. Massouridès E, Polentes J, Mangeot PE, Mournetas V, Nectoux J, Deburgrave N, et al. Dp412e: A novel human embryonic

dystrophin isoform induced by BMP4 in early differentiated cells. Skelet Muscle [Internet]. 2015 Dec 14 [cited 2017 Feb 27];5(1):40. Available from: http://www.skeletalmusclejournal.com/content/5/1/40

16. Nesmith AP, Wagner MA, Pasqualini FS, B OB, Pincus MJ, August PR, et al. A human in vitro model of Duchenne muscular dystrophy muscle formation and contractility. J Cell Biol. 2016;215(1):47–56.

17. Shoji E, Sakurai H, Nishino T, Nakahata T, Heike T, Awaya T, et al. Early pathogenesis of Duchenne muscular dystrophy modelled in patient-derived human induced pluripotent stem cells. Sci Rep. 2015;5:12831.

18. Choi IY, Lim HT, Estrellas K, Mula J, Cohen T V., Zhang Y, et al. Concordant but Varied Phenotypes among Duchenne Muscular Dystrophy Patient-Specific Myoblasts Derived using a Human iPSC-Based Model. Cell Rep. 2016;15(10):2301–12.

19. Chal J, Oginuma M, Al Tanoury Z, Gobert B, Sumara O, Hick A, et al. Differentiation of pluripotent stem cells to muscle fiber to model Duchenne muscular dystrophy. Nat Biotechnol. 2015;33(9):962–9.

20. Young CS, Hicks MR, Ermolova N V, Nakano H, Jan M, Younesi S, et al. A Single {CRISPR-Cas9} Deletion Strategy that Targets the Majority of {DMD} Patients Restores Dystrophin Function in {hiPSC-Derived} Muscle Cells. Cell Stem Cell. 2016;18(4):533–40.

21. Hicks MR, Hiserodt J, Paras K, Fujiwara W, Eskin A, Jan M, et al. {ERBB3} and {NGFR} mark a distinct skeletal muscle progenitor cell in human development and {hPSCs.}. Nat Cell Biol. 2018;20(1):46–57.

22. Kodaka Y, Rabu G, Asakura A. Skeletal Muscle Cell Induction from Pluripotent Stem Cells. Stem Cells Int. 2017;2017:1376151.

23. Caron L, Kher D, Lee KL, McKernan R, Dumevska B, Hidalgo A, et al. A Human Pluripotent Stem Cell Model of Facioscapulohumeral Muscular Dystrophy-Affected Skeletal Muscles. Stem Cells Transl Med. 2016;5(9):1145–61.

24. Shelton M, Metz J, Liu J, Carpenedo RL, Demers S-PP, Stanford WL, et al. Derivation and expansion of {PAX7-positive} muscle progenitors from human and mouse embryonic stem cells. Stem Cell Reports. 2014;3(3):516–29.

25. Xi H, Fujiwara W, Gonzalez K, Jan M, Liebscher S, Van Handel B, et al. {In~Vivo} Human Somitogenesis Guides Somite Development from {hPSCs.}. Cell Rep. 2017;18(6):1573–85.

26. Monaco AP, Neve RL, Chris C-F, Bertelson CJ, Kurnit DM, Kunkel LM. Isolation of candidate {cDNAs} for portions of the Duchenne muscular dystrophy gene. Nature. 1986;323(6089):646–50.

27. Byers TJ, Lidov HGW, Kunkel LM. An alternative dystrophin transcript specific to peripheral nerve. Nat Genet. 1993;4(1):ng0593-77.

28. Lidov HG, Selig S, Kunkel LM. Dp140: a novel 140 {kDa} {CNS} transcript from the dystrophin locus. Hum Mol Genet. 1995;4(3):329–35.

29. Górecki DC, Monaco AP, Derry JM, Walker AP, Barnard EA, Barnard PJ. Expression of four alternative dystrophin transcripts in brain regions regulated by different promoters. Hum Mol Genet. 1992;1(7):505–10.

30. D'souza VN, Man NT, Morris GE, Karges W, Pillers DAM, Ray PN. A novel dystrophin isoform is required for normal retinal electrophysiology. Hum Mol Genet. 1995;4(5):837–42.

31. Nudel U, Zuk D, Einat P, Zeelon E, Levy Z, Neuman S, et al. Duchenne muscular dystrophy gene product is not identical in muscle and brain. Nature. 1989;337(6202):337076a0.

32. Heikinheimo M, Scandrett JM, Wilson DB. Localization of Transcription Factor GATA-4 to Regions of the Mouse Embryo Involved in Cardiac Development. Dev Biol. 1994;164(2):361–73.

33. Pfeffer PL, Gerster T, Lun K, Brand M, Busslinger M. Characterization of three novel members of the zebrafish Pax2/5/8 family: dependency of Pax5 and Pax8 expression on the Pax2.1 (noi) function. Development [Internet]. 1998;125(16):3063–74. Available from: http://www.ncbi.nlm.nih.gov/pubmed/9671580

34. Chapman DL, Cooper-Morgan A, Harrelson Z, Papaioannou VE. Critical role for Tbx6 in mesoderm specification in the mouse embryo. Mech Dev. 2003;120(7):837–47.

35. Hart AH, Hartley L, Sourris K, Stadler ES, Li R, Stanley EG, et al. Mixl1 is required for axial mesendoderm morphogenesis and patterning in the murine embryo. Development [Internet]. 2002;129(15):3597–608. Available from: http://www.ncbi.nlm.nih.gov/pubmed/12117810

36. Kanai-Azuma M, Kanai Y, Gad JM, Tajima Y, Taya C, Kurohmaru M, et al. Depletion of definitive gut endoderm in Sox17-null mutant mice. Development [Internet]. 2002;129(10):2367–79. Available from: http://www.ncbi.nlm.nih.gov/pubmed/11973269

37. Rex M, Orme A, Uwanogho D, Tointon K, Wigmore PM, Sharpe PT, et al. Dynamic expression of chicken Sox2 and Sox3 genes in ectoderm induced to form neural tissue. Dev Dyn. 1997;209(3):323–32.

38. Machon O, Masek J, Machonova O, Krauss S, Kozmik Z. Meis2 is essential for cranial and cardiac neural crest development. BMC Dev Biol. 2015;15(1):40.

39. Laing NG, Dye DE, Wallgren-Pettersson C, Richard G, Monnier N, Lillis S, et al. Mutations and polymorphisms of the skeletal muscle α-actin gene (ACTA1). Hum Mutat. 2009;30(9):1267–77.

40. Kardon G, Heanue TA, Tabin CJ. Pax3 and Dach2 positive regulation in the developing somite. Dev Dyn. 2002;224(3):350–5.

41. Pereira FA, Yuhong Q, Zhou G, Tsai MJ, Tsai SY. The orphan nuclear receptor COUP-TFII is required for angiogenesis and heart development. Genes Dev. 1999;13(8):1037–49.

42. Mitsiadis TA, Salmivirta M, Muramatsu T, Muramatsu H, Rauvala H, Lehtonen E, et al. Expression of the heparin-binding cytokines, midkine (MK) and HB-GAM (pleiotrophin) is associated with epithelial-mesenchymal interactions during fetal development and organogenesis. Development [Internet]. 1995;121(1):37–51. Available from: http://www.ncbi.nlm.nih.gov/pubmed/7867507

43. Yang XM, Vogan K, Gros P, Park M. Expression of the met receptor tyrosine kinase in muscle progenitor cells in somites and limbs is absent in Splotch mice. Development [Internet]. 1996;122(7):2163–71. Available from: http://www.ncbi.nlm.nih.gov/pubmed/8681797

44. Sasaki H, Ferguson-Smith AC, Shum AS, Barton SC, Surani MA. Temporal and spatial regulation of H19 imprinting in normal and uniparental mouse embryos. Development [Internet]. 1995;121(12):4195–202. Available from:

http://www.ncbi.nlm.nih.gov/pubmed/8575319

45. Borycki AG, Mendham L, Emerson CP. Control of somite patterning by Sonic hedgehog and its downstream signal response genes. Development [Internet]. 1998;125(4):777–90. Available from: http://www.ncbi.nlm.nih.gov/pubmed/9435297

46. Lee CS, Buttitta L, Fan C-M. Evidence that the {WNT-inducible} growth arrest-specific gene 1 encodes an antagonist of sonic hedgehog signaling in the somite. Proc Natl Acad Sci. 2001;98(20):11347–52.

47. McMahon AR, Merzdorf CS. Expression of the zic1, zic2, zic3, and zic4 genes in early chick embryos. BMC Res Notes. 2010;3(1):167.

48. Bladt F, Riethmacher D, Isenmann S, Aguzzi A, Birchmeier C. Essential role for the c-met receptor in the migration of myogenic precursor cells into the limb bud. Nature. 1995;376(6543):768–71.

49. Swartz ME, Eberhart J, Pasquale EB, Krull CE. EphA4/ephrin-A5 interactions in muscle precursor cell migration in the avian forelimb. Development [Internet]. 2001;128(23):4669–80. Available from: http://www.ncbi.nlm.nih.gov/pubmed/11731448

50. Schäfer K, Braun T. Early specification of limb muscle precursor cells by the homeobox gene Lbx1h. Nat Genet. 1999;23(2):ng1099_213.

51. Crossley PH, Minowada G, MacArthur CA, Martin GR. Roles for FGF8 in the induction, initiation, and maintenance of chick limb development. Cell. 1996;84(1):127–36.

52. Stewart RA, Arduini BL, Berghmans S, George RE, Kanki JP, Henion PD, et al. Zebrafish foxd3 is selectively required for neural crest specification, migration and survival. Dev Biol. 2006;292(1):174–88.

53. Deutsch U, Dressler GR, Gruss P. Pax 1, a member of a paired box homologous murine gene family, is expressed in segmented structures during development. Cell. 1988;53(4):617–25.

54. Buchner G, Broccoli V, Bulfone A, Orfanelli U, Gattuso C, Ballabio A, et al. {MAEG,} an {EGF-repeat} containing gene, is a new marker associated with dermatome specification and morphogenesis of its derivatives. Mech Dev. 2000;98(1–2):179–82.

55. Xu X-M, Fisher DA, Zhou L, White FA, Ng S, Snider WD, et al. The Transmembrane Protein Semaphorin {6A} Repels Embryonic Sympathetic Axons. J Neurosci. 2000;20(7):2638–48.

56. Davis RL, Weintraub H, Lassar AB. Expression of a single transfected cDNA converts fibroblasts to myoblasts. Cell. 1987;51(6):987–1000.

57. Donalies M, Cramer M, Ringwald M, A S-P. Expression of M-cadherin, a member of the cadherin multigene family, correlates with differentiation of skeletal muscle cells. Proc Natl Acad Sci. 1991;88(18):8024–8.

58. Gahlmann R, Kedes L. Cloning, structural analysis, and expression of the human fast twitch skeletal muscle troponin C gene. J Biol Chem. 1990;265(21):12520–8.

59. Roberds SL, Anderson RD, Ibraghimov-Beskrovnaya O, Campbell KP. Primary structure and muscle-specific expression of the 50-kDa dystrophin-associated glycoprotein (adhalin). J Biol Chem [Internet]. 1993;268(32):23739–42. Available from:

http://www.ncbi.nlm.nih.gov/pubmed/8226900

60. MacKenzie AE, Korneluk RG, Zorzato F, Fujii J, Phillips M, Iles D, et al. The human ryanodine receptor gene: its mapping to 19q13.1, placement in a chromosome 19 linkage group, and exclusion as the gene causing myotonic dystrophy. Am J Hum Genet [Internet]. 1990;46(6):1082–9. Available from: http://www.ncbi.nlm.nih.gov/pubmed/1971150%0Ahttp://www.pubmedcentral.nih.gov/articlerender.fcgi?artid=PMC1683814

61. Greco S, De Simone M, Colussi C, Zaccagnini G, Fasanaro P, Pescatori M, et al. Common {micro-RNA} signature in skeletal muscle damage and regeneration induced by Duchenne muscular dystrophy and acute ischemia. {FASEB} J. 2009;23(10):3335–46.

62. Milet C, Duprez D. The Mkx homeoprotein promotes tenogenesis in stem cells and improves tendon repair. Ann Transl Med. 2015;3(Suppl 1):S33.

63. Lefebvre V, Li P, De Crombrugghe B. A new long form of Sox5 (L-Sox5), Sox6 and Sox9 are coexpressed in chondrogenesis and cooperatively activate the type II collagen gene. EMBO J. 1998;17(19):5718–33.

64. NODA M, DENHARDT DT. Regulation of Osteopontin Gene Expression in Osteoblasts. Ann N Y Acad Sci. 1995;760(1):242–8.

65. Atala A. Re: Sall1 Maintains Nephron Progenitors and Nascent Nephrons by Acting as Both an Activator and a Repressor: Editorial Comment. J Urol. 2015;194(2):592–3.

66. Lytton J, DH M. Molecular cloning of {cDNAs} from human kidney coding for two alternatively spliced products of the cardiac {Ca2+-ATPase} gene. J Biol Chem. 1988;263(29):15024–31.

67. Yoshida M, Ozawa E. Glycoprotein complex anchoring dystrophin to sarcolemma. J Biochem. 1990;108(5):748–52.

68. Chen JF, Mandel EM, Thomson JM, Wu Q, Callis TE, Hammond SM, et al. The role of microRNA-1 and microRNA-133 in skeletal muscle proliferation and differentiation. Nat Genet. 2006;38(2):228–33.

69. Hak KK, Yong SL, Sivaprasad U, Malhotra A, Dutta A. Muscle-specific microRNA miR-206 promotes muscle differentiation. J Cell Biol. 2006;174(5):677–87.

70. Hasty P, Bradley A, Morris JH, Edmondson DG, Venuti JM, Olson EN, et al. Muscle deficiency and neonatal death in mice with a targeted mutation in the myogenin gene. Nature. 1993;364(6437):364501a0.

71. Vignier N, Moghadaszadeh B, Gary F, Beckmann J, Mayer U, Guicheney P. Structure, genetic localization, and identification of the cardiac and skeletal muscle transcripts of the human integrin α7 gene (ITGA7). Biochem Biophys Res Commun. 1999;260(2):357–64.

72. Newey SE, Howman E V., Ponting CP, Benson MA, Nawrotzki R, Loh NY, et al. Syncoilin, a Novel Member of the Intermediate Filament Superfamily That Interacts with α-Dystrobrevin in Skeletal Muscle. J Biol Chem. 2001;276(9):6645–55.

73. WU Q-L, JHA PK, RAYCHOWDHURY MK, DU Y, LEAVIS PC, SARKAR S. Isolation and Characterization of Human Fast Skeletal β Troponin T cDNA: Comparative Sequence Analysis of Isoforms and Insight into the Evolution of Members of a Multigene Family. DNA Cell Biol. 2009;13(3):217–33.

855 74. Bernick EP, Zhang PJ, Du S. Knockdown and overexpression of Unc-45b result in defective myofibril organization in skeletal
856 muscles of zebrafish embryos. BMC Cell Biol. 2010;11(1):70.

857 75. Li H, Randall WR, Du S-J. skNAC (skeletal Naca), a muscle-specific isoform of Naca (nascent polypeptide-associated complex
858 alpha), is required for myofibril organization. FASEB J. 2009;23(6):1988–2000.

859 76. DeChiara TM, Bowen DC, Valenzuela DM, Simmons M V., Poueymirou WT, Thomas S, et al. The receptor tyrosine kinase MuSK is
860 required for neuromuscular junction formation in vivo. Cell. 1996;85(4):501–12.

861 77. Okada K, Inoue A, Okada M, Murata Y, Kakuta S, Jigami T, et al. The Muscle Protein Dok-7 Is Essential for Neuromuscular
862 Synaptogenesis. Science (80-). 2006;312(5781):1802–5.

863 78. Ilene K-M, Travis M, Blau H, Leinwand LA. Expression and {DNA} sequence analysis of a human embryonic skeletal muscle mvosin
864 heavy chain gene. Nucleic Acids Res. 1989;17(15):6167–79.

865 79. Weiss A, Schiaffino S, Leinwand LA. Comparative sequence analysis of the complete human sarcomeric myosin heavy chain
866 family: implications for functional {diversity11Edited} by J. Karn. J Mol Biol. 1999;290(1):61–75.

867 80. Strohman RC, J M-E, Glass CA, Matsuda R. Human fetal muscle and cultured myotubes derived from it contain a fetal-specific
868 myosin light chain. Science (80-). 1983;221(4614):955–7.

869 81. Collins C, Hayden MR, Schappert K. The genomic organization of a novel regulatory myosin light chain gene (MYL5) that maps to
870 chromosome 4p16.3 and shows different patterns of expression between primates. Hum Mol Genet. 1992;1(9):727–33.

871 82. Type IIx myosin heavy chain transcripts are expressed in type IIb fibers of human skeletal muscle. Am J Physiol - Cell Physiol.
872 1994;267(6 36-6):C1723-8.

873 83. Rotwein P, Pollock KM, Watson M, Milbrandt JD. Insulin-like growth factor gene expression during rat embryonic development.
874 Endocrinology. 1987;121(6):2141–4.

875 84. Andersen DC, Laborda J, Baladron V, Kassem M, Sheikh SP, Jensen CH. Dual role of delta-like 1 homolog (DLK1) in skeletal muscle
876 development and adult muscle regeneration. Development. 2013;140(18):3743–53.

877 85. Noguchi S, EM M, Othmane BK, Hagiwara Y, Mizuno Y, Yoshida M, et al. Mutations in the dystrophin-associated protein gamma-
878 sarcoglycan in chromosome 13 muscular dystrophy. Sci New York N Y. 1995;270(5237):819–22.

879 86. Campbell KP, Leung AT, Sharp AH. The biochemistry and molecular biology of the dihydropyridine-sensitive calcium channel.
880 Trends Neurosci. 1988;11(10):425–30.

881 87. A fourth human MEF2 transcription factor, hMEF2D, is an early marker of the myogenic lineage. Development.
882 1993;118(4):1095–106.

883 88. Gautam M, Noakes PG, Mudd J, Nichol M, Chu GC, Sanes JR, et al. Failure of postsynaptic specialization to develop at
884 neuromuscular junctions of rapsyn-deficient mice. Nature. 1995;377(6546):377232a0.

885 89. Dawson DM, Eppenberger HM, Eppenberger ME. Multiple Molecular Forms of Creatine Kinases. Ann N Y Acad Sci.

1968;151(1):616–26.

90. van Rooij E, Sutherland LB, Qi X, Richardson JA, Hill J, Olson EN. Control of {Stress-Dependent} Cardiac Growth and Gene Expression by a {MicroRNA}. Science (80-). 2007;316(5824):575–9.

91. Hailstones D, Barton P, P C-T, Sasse S, Sutherland C, Hardeman E, et al. Differential regulation of the atrial isoforms of the myosin light chains during striated muscle development. J Biol Chem. 1992;267(32):23295–300.

92. Marx SO, Reiken S, Hisamatsu Y, Jayaraman T, Burkhoff D, Rosemblit N, et al. PKA Phosphorylation Dissociates FKBP12.6 from the Calcium Release Channel (Ryanodine Receptor). Cell. 2004;101(4):365–76.

93. Kuro-o M, Nagai R, Tsuchimochi H, Katoh H, Yazaki Y, Ohkubo A, et al. Developmentally regulated expression of vascular smooth muscle myosin heavy chain isoforms. J Biol Chem. 1989;264(31):18272–5.

94. Gimona M, Herzog M, Vandekerckhove J, Small JV. Smooth muscle specific expression of calponin. FEBS Lett. 1990;274(1–2):159–62.

95. Eglen RM, Reddy H, Watson N, Challiss RAJ. Muscarinic acetylcholine receptor subtypes in smooth muscle. Trends Pharmacol Sci. 1994;15(4):114–9.

96. Ajima R, Akazawa H, Kodama M, Takeshita F, Otsuka A, Kohno T, et al. Deficiency of Myo18B in mice results in embryonic lethality with cardiac myofibrillar aberrations. Genes to Cells. 2008;13(10):987–99.

97. Heidmann O, Buonanno A, Geoffroy B, Robert B, Guenet JL, Merlie JP, et al. Chromosomal localization of muscle nicotinic acetylcholine receptor genes in the mouse. Science (80-). 1986;234(4778):866–8.

98. Ueno T, Tanaka K, Kaneko K, Taga Y, Sata T, Irie S, et al. Enhancement of procollagen biosynthesis by p180 through augmented ribosome association on the endoplasmic reticulum in response to stimulated secretion. J Biol Chem. 2010;285(39):29941–50.

99. Hautala T, Byers MG, Eddy RL, Shows TB, Kivirikko KI, Myllyla R. Cloning of human lysyl hydroxylase: Complete cDNA-derived amino acid sequence and assignment of the gene (PLOD) to chromosome 1p36.3→p36.2. Genomics. 1992;13(1):62–9.

100. Valtavaara M, Papponen H, Pirttilä AM, Hiltunen K, Helander H, Myllylä R. Cloning and characterization of a novel human lysyl hydroxylase isoform highly expressed in pancreas and muscle. J Biol Chem. 1997;272(11):6831–4.

101. Martens JHA, Verlaan M, Kalkhoven E, Zantema A. Cascade of Distinct Histone Modifications during Collagenase Gene Activation. Mol Cell Biol. 2003;23(5):1808–16.

102. Long DA, Price KL, Ioffe E, Gannon CM, Gnudi L, White KE, et al. Angiopoietin-1 therapy enhances fibrosis and inflammation following folic acid-induced acute renal injury. Kidney Int. 2008;74(3):300–9.

103. Lipson KE, Wong C, Teng Y, Spong S. CTGF is a central mediator of tissue remodeling and fibrosis and its inhibition can reverse the process of fibrosis. Fibrogenesis Tissue Repair [Internet]. 2012;5(S1):S24. Available from: https://fibrogenesis.biomedcentral.com/articles/10.1186/1755-1536-5-S1-S24

104. Fragiadaki M, Witherden AS, Kaneko T, Sonnylal S, Pusey CD, George B-G, et al. Interstitial fibrosis is associated with increased

{COL1A2} transcription in {AA-injured} renal tubular epithelial cells in vivo. Matrix Biol. 2011;30(7–8):396–403.

105. Hemmann S, Graf J, Roderfeld M, Roeb E. Expression of {MMPs} and {TIMPs} in liver fibrosis – a systematic review with special emphasis on anti-fibrotic strategies. J Hepatol. 2007;46(5):955–75.

106. Duisters RF, Tijsen AJ, Schroen B, Leenders JJ, Lentink V, Van Der Made I, et al. MiR-133 and miR-30 Regulate connective tissue growth factor: Implications for a role of micrornas in myocardial matrix remodeling. Circ Res. 2009;104(2):170–8.

107. Vidal B, Serrano AL, Tjwa M, Suelves M, Ardite E, Mori R, et al. Fibrinogen drives dystrophic muscle fibrosis via a {TGFβ/alternative} macrophage activation pathway. Gene Dev. 2008;22(13):1747–52.

108. Timpani CA, Hayes A, Rybalka E. Revisiting the dystrophin-ATP connection: How half a century of research still implicates mitochondrial dysfunction in Duchenne Muscular Dystrophy aetiology. Med Hypotheses. 2015;85(6):1021–33.

109. Šileikyte J, Blachly-Dyson E, Sewell R, Carpi A, Menabò R, Di Lisa F, et al. Regulation of the mitochondrial permeability transition pore by the outer membrane does not involve the peripheral benzodiazepine receptor (translocator protein of 18 kDa (TSPO)). J Biol Chem. 2014;289(20):13769–81.

110. Emery AE, Burt D. Intracellular calcium and pathogenesis and antenatal diagnosis of Duchenne muscular dystrophy. Br Med J. 1980;280(6211):355–7.

111. Shkryl VM, Martins AS, Ullrich ND, Nowycky MC, Niggli E, Shirokova N. Reciprocal amplification of ROS and Ca2+ signals in stressed mdx dystrophic skeletal muscle fibers. Pflugers Arch Eur J Physiol. 2009;458(5):915–28.

112. Whitehead NP, Yeung EW, Froehner SC, Allen DG. Skeletal muscle NADPH oxidase is increased and triggers stretch-induced damage in the mdx mouse. PLoS One. 2010;5(12):e15354.

113. Rodriguez MC, Tarnopolsky MA. Patients with dystrophinopathy show evidence of increased oxidative stress. Free Radic Biol Med. 2003;34(9):1217–20.

114. Scholte HR, Busch HFM. Early changes of muscle mitochondria in duchenne dystrophy Partition and activity of mitochondrial enzymes in fractionated muscle of unaffected boys and adults and patients. J Neurol Sci. 1980;45(2–3):217–34.

115. Sharma U, Atri S, Sharma MC, Sarkar C, Jagannathan NR. Skeletal muscle metabolism in Duchenne muscular dystrophy {(DMD):} an in-vitro proton {NMR} spectroscopy study. Magn Reson Imaging. 2003;21(2):145–53.

116. Lemos DR, Babaeijandaghi F, Low M, Chang C-K, Lee ST, Fiore D, et al. Nilotinib reduces muscle fibrosis in chronic muscle injury by promoting {TNF-mediated} apoptosis of fibro/adipogenic progenitors. Nat Med. 2015;21(7):786–94.

117. Villalta AS, Nguyen HX, Deng B, Gotoh T, Tidball JG. Shifts in macrophage phenotypes and macrophage competition for arginine metabolism affect the severity of muscle pathology in muscular dystrophy. Hum Mol Genet. 2009;18(3):482–96.

118. Desguerre I, Mayer M, Leturcq F, Barbet J-P, Gherardi RK, Christov C. Endomysial Fibrosis in Duchenne Muscular Dystrophy: A Marker of Poor Outcome Associated With Macrophage Alternative Activation. J Neuropathol Exp Neurol. 2009;68(7):762–73.

119. Fusako S-T, Narita A, Masuda S, Wakamatsu T, Watanabe N, Nishiyama T, et al. Premyogenic progenitors derived from human

pluripotent stem cells expand in floating culture and differentiate into transplantable myogenic progenitors. Sci Rep-uk. 2018;8(1):6555.

120. Matsumura K, Tome FMS, Ionasescu V, Ervasti JM, Anderson RD, Romero NB, et al. Deficiency of dystrophin-associated proteins in Duchenne muscular dystrophy patients lacking COOH-terminal domains of dystrophin. J Clin Invest. 1993;92(2):866–71.

121. Yuasa K, Hagiwara Y, Ando M, Nakamura A, Takeda S, Hijikata T. {MicroRNA-206} is highly expressed in newly formed muscle fibers: implications regarding potential for muscle regeneration and maturation in muscular dystrophy. Cell Struct Funct. 2008;33(2):163–9.

122. Cullen MJ, Fulthorpe JJ. Stages in fibre breakdown in duchenne muscular dystrophy An electron-microscopic study. J Neurol Sci. 1975;24(2):179–200.

123. Brouilly N, Lecroisey C, Martin E, Pierson L, Mariol MC, Mounier N, et al. Ultra-structural time-course study in the C. elegans model for Duchenne muscular dystrophy highlights a crucial role for sarcomere-anchoring structures and sarcolemma integrity in the earliest steps of the muscle degeneration process. Hum Mol Genet. 2015;24(22):6428–45.

124. Consolino CM, Brooks S V. Susceptibility to sarcomere injury induced by single stretches of maximally activated muscles of mdx mice. J Appl Physiol Bethesda Md 1985. 2004;96(2):633–8.

125. Kong J, Anderson JE. Dystrophin is required for organizing large acetylcholine receptor aggregates. Brain Res. 1999;839(2):298–304.

126. Kong J, Yang L, Li Q, Cao J, Yang J, Chen F, et al. The absence of dystrophin rather than muscle degeneration causes acetylcholine receptor cluster defects in dystrophic muscle. Neuroreport. 2012;23(2):82–7.

127. Bell CD, Conen PE. Histopathological changes in Duchenne muscular dystrophy. J Neurol Sci. 1968;7(3):529–44.

128. Haddix SG, il Lee Y, Kornegay JN, Thompson WJ. Cycles of myofiber degeneration and regeneration lead to remodeling of the neuromuscular junction in two mammalian models of Duchenne muscular dystrophy. PLoS One. 2018;13(10):e0205926.

129. Luz MAM, Marques MJ, Neto SH. Impaired regeneration of dystrophin-deficient muscle fibers is caused by exhaustion of myogenic cells. Braz J Med Biol Res. 2002;35(6):691–5.

130. Zhou L, Porter JD, Cheng G, Gong B, Hatala DA, Merriam AP, et al. Temporal and spatial {mRNA} expression patterns of {TGF-beta1,} 2, 3 and {TbetaRI,} {II,} {III} in skeletal muscles of mdx mice. Neuromuscul Disord Nmd. 2005;16(1):32–8.

131. Bernasconi P, Torchiana E, Confalonieri P, Brugnoni R, Barresi R, Mora M, et al. Expression of transforming growth factor-beta 1 in dystrophic patient muscles correlates with fibrosis. Pathogenetic role of a fibrogenic cytokine. J Clin Invest. 1995;96(2):1137–44.

132. Takahashi K, Tanabe K, Ohnuki M, Narita M, Ichisaka T, Tomoda K, et al. Induction of Pluripotent Stem Cells from Adult Human Fibroblasts by Defined Factors. Cell. 2007;131(5):861–72.

133. DREYFUS JC, SCHAPIRA G, SCHAPIRA F. Biochemical study of muscle in progressive muscular dystrophy. J Clin Invest.

1954;33(5):794–7.

134. Ascah A, Khairallah M, Daussin F, Bourcier-Lucas C, Godin R, Allen BG, et al. Stress-induced opening of the permeability transition pore in the dystrophin-deficient heart is attenuated by acute treatment with sildenafil. Am J Physiol Circ Physiol. 2011;300(1):H144–53.

135. Pauly M, Daussin F, Burelle Y, Li T, Godin R, Fauconnier J, et al. AMPK activation stimulates autophagy and ameliorates muscular dystrophy in the mdx mouse diaphragm. Am J Pathol. 2012;181(2):583–92.

136. M PC. {HISTOPATHOLOGICAL} {FEATURES} {OF} {MUSCLE} {IN} {THE} {PRECLINICAL} {STAGES} {OF} {MUSCULAR} {DYSTROPHY}. Brain. 1962;85(1):109–20.

137. Bradley WG, Hudgson P, Larson PF, Papapetropoulos TA, Jenkison M. Structural changes in the early stages of Duchenne muscular dystrophy. J Neurol Neurosurg Psychiatry. 1972;35(4):451.

138. Rau F, Freyermuth F, Fugier C, Villemin JP, Fischer MC, Jost B, et al. Misregulation of miR-1 processing is associated with heart defects in myotonic dystrophy. Nat Struct Mol Biol. 2011;18(7):840–5.

139. Singh A, Happel C, Manna SK, George A-M, Carrerero J, Kumar S, et al. Transcription factor {NRF2} regulates {miR-1} and {miR-206} to drive tumorigenesis. J Clin Invest. 2013;123(7):2921–34.

140. Zhang X, Zuo X, Yang B, Li Z, Xue Y, Zhou Y, et al. MicroRNA directly enhances mitochondrial translation during muscle differentiation. Cell. 2014;158(3):607–19.

141. Fry CS, Kirby TJ, Kosmac K, McCarthy JJ, Peterson CA. Myogenic Progenitor Cells Control Extracellular Matrix Production by Fibroblasts during Skeletal Muscle Hypertrophy. Cell Stem Cell. 2017;20(1):56–69.

142. Blau HM, Webster C, Pavlath GK. Defective myoblasts identified in Duchenne muscular dystrophy. Proc Natl Acad Sci. 1983;80(15):4856–60.

143. Bovolenta M, Erriquez D, Valli E, Brioschi S, Scotton C, Neri M, et al. The DMD Locus Harbours Multiple Long Non-Coding RNAs Which Orchestrate and Control Transcription of Muscle Dystrophin mRNA Isoforms. PLoS One. 2012;7(9).

144. Ervasti JM, Campbell KP. A role for the dystrophin-glycoprotein complex as a transmembrane linker between laminin and actin. J Cell Biol. 1993;122(4):809–23.

145. Muntoni F, Melis MA, Ganau A, Dubowitz V. Transcription of the dystrophin gene in normal tissues and in skeletal muscle of a family with X-linked dilated cardiomyopathy. Am J Hum Genet. 1995;56(1):151–7.

146. Warner LE. Expression of Dp260 in muscle tethers the actin cytoskeleton to the dystrophin-glycoprotein complex and partially prevents dystrophy. Hum Mol Genet. 2002;11(9):1095–105.

147. Doorenweerd N, Mahfouz A, Van Putten M, Kaliyaperumal R, T'Hoen PAC, Hendriksen JGM, et al. Timing and localization of human dystrophin isoform expression provide insights into the cognitive phenotype of Duchenne muscular dystrophy. Sci Rep. 2017;7(1).

148. Lu-Nguyen N, Ferry A, Schnell FJ, Hanson GJ, Popplewell L, Dickson G, et al. Functional muscle recovery following dystrophin and myostatin exon splice modulation in aged mdx mice. Hum Mol Genet. 2019;

149. Peccate C, Mollard A, Le Hir M, Julien L, McClorey G, Jarmin S, et al. Antisense pre-treatment increases gene therapy efficacy in dystrophic muscles. Hum Mol Genet. 2016;25(16):3555–63.

150. Morales MG, Gutierrez J, Cabello-Verrugio C, Cabrera D, Lipson KE, Goldschmeding R, et al. Reducing CTGF/CCN2 slows down mdx muscle dystrophy and improves cell therapy. Hum Mol Genet. 2013;22(24):4938–51.

151. Gatliff J, Campanella M. {TSPO:} kaleidoscopic {18-kDa} amid biochemical pharmacology, control and targeting of mitochondria. Biochem J. 2016;473(2):107–21.

152. Köster J, Rahmann S. Snakemake—a scalable bioinformatics workflow engine. Bioinformatics. 2012;28(19):2520–2.

153. Dobin A, Davis C a, Schlesinger F, Drenkow J, Zaleski C, Jha S, et al. STAR: ultrafast universal RNA-seq aligner. Bioinformatics [Internet]. 2013 Jan 1 [cited 2014 Jul 13];29(1):15–21. Available from: http://www.pubmedcentral.nih.gov/articlerender.fcgi?artid=3530905&tool=pmcentrez&rendertype=abstract

154. Wang L, Wang S, Li W. RSeQC: quality control of RNA-seq experiments. Bioinformatics [Internet]. 2012 Aug 15 [cited 2017 Jul 6];28(16):2184–5. Available from: https://academic.oup.com/bioinformatics/article-lookup/doi/10.1093/bioinformatics/bts356

155. Liao Y, Smyth GK, Shi W. FeatureCounts: An efficient general purpose program for assigning sequence reads to genomic features. Bioinformatics [Internet]. 2014 Apr 1 [cited 2017 Jul 6];30(7):923–30. Available from: http://www.ncbi.nlm.nih.gov/pubmed/24227677

156. Ewels P, Magnusson M, Lundin S, Käller M. MultiQC: Summarize analysis results for multiple tools and samples in a single report. Bioinformatics [Internet]. 2016 Oct 1 [cited 2017 Jul 6];32(19):3047–8. Available from: https://academic.oup.com/bioinformatics/article-lookup/doi/10.1093/bioinformatics/btw354

157. Love MI, Huber W, Anders S. Moderated estimation of fold change and dispersion for RNA-seq data with DESeq2. Genome Biol [Internet]. 2014;15(12):550. Available from: http://genomebiology.biomedcentral.com/articles/10.1186/s13059-014-0550-8

158. Durinck S, Spellman PT, Birney E, Huber W. Mapping identifiers for the integration of genomic datasets with the R/ Bioconductor package biomaRt. Nat Protoc [Internet]. 2009 [cited 2019 Jun 12];4(8):1184–91. Available from: http://www.ncbi.nlm.nih.gov/pubmed/19617889

159. Kolesnikov N, Hastings E, Keays M, Melnichuk O, Tang AY, Williams E, et al. {ArrayExpress} update—simplifying data submissions. Nucleic Acids Res. 2015;43(D1):D1113–6.

160. Schmieder R, Edwards R. Quality control and preprocessing of metagenomic datasets. Bioinformatics. 2011;27(6):863–4.

161. Martin M. Cutadapt removes adapter sequences from high-throughput sequencing reads. Embnet J. 2011;17(1):10–2.

162. Amrhein V, Greenland S, Blake M. Scientists rise up against statistical significance. Nature. 2019;567(7748):305–7.

163. Garnier S. viridis: Default Color Maps from “matplotlib”. R package version 0.5.1. 2018; Available from: https://cran.r-

project.org/package=viridis

164. Simko TW and V. R package "corrplot": Visualization of a Correlation Matrix (Version 0.84). 2017; Available from: https://github.com/taiyun/corrplot

165. Gregory R. Warnes, Ben Bolker, Lodewijk Bonebakker, Robert Gentleman, Wolfgang Huber Andy Liaw, Thomas Lumley M, Maechler, Arni Magnusson, Steffen Moeller MS and BV. gplots: Various R Programming Tools for Plotting Data. R package version 3.0.1. 2016; Available from: https://cran.r-project.org/package=gplots

166. Fresno C, Fernández EA. {RDAVIDWebService:} a versatile R interface to {DAVID}. Bioinformatics. 2013;29(21):2810–1.

167. Vizcaíno J, Csordas A, del-Toro, Noemi, Dianes JA, Griss J, Lavidas I, et al. 2016 update of the {PRIDE} database and its related tools. Nucleic Acids Res. 2016;44(D1):D447–56.

Figure 1

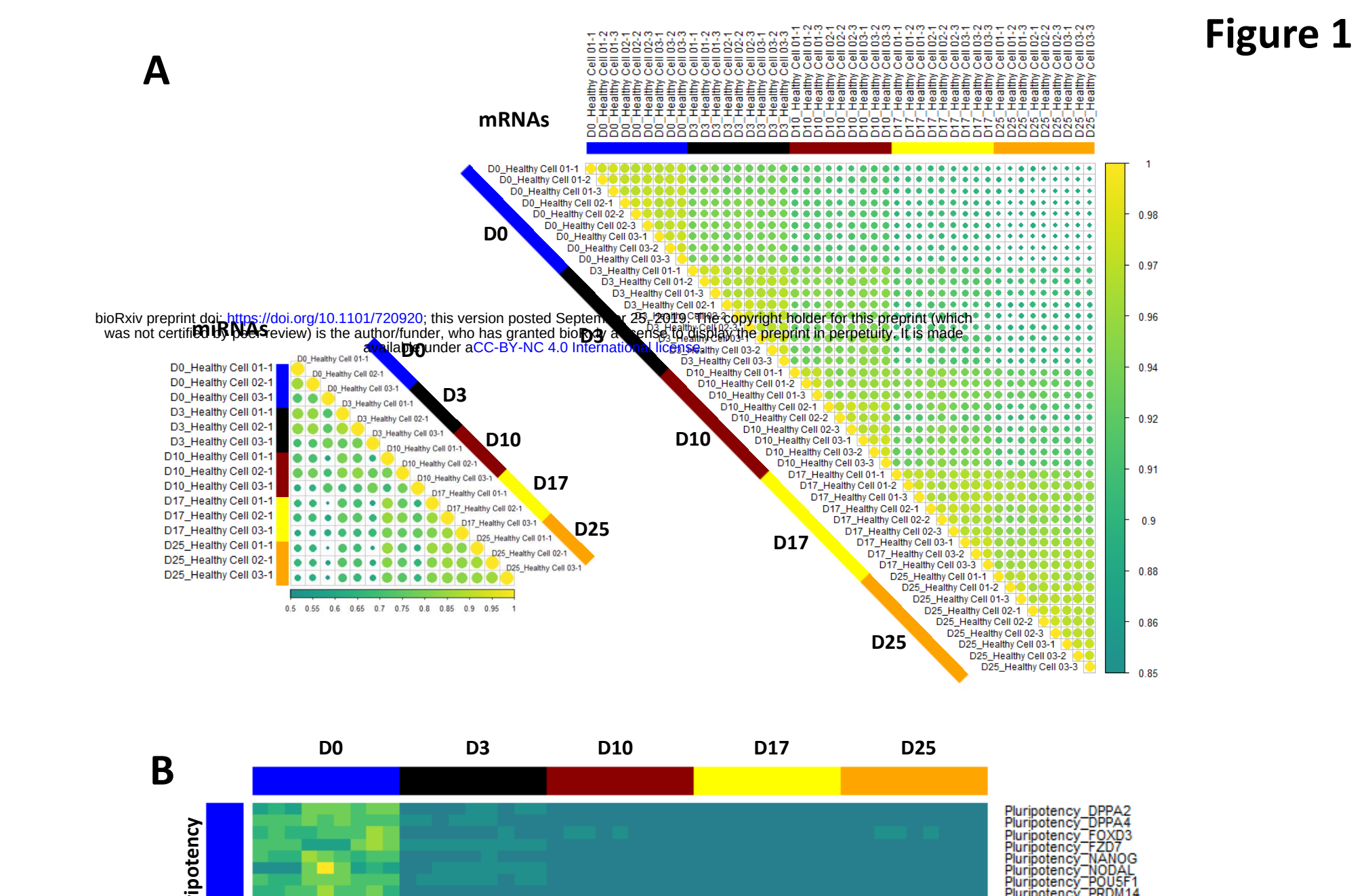

Figure 2

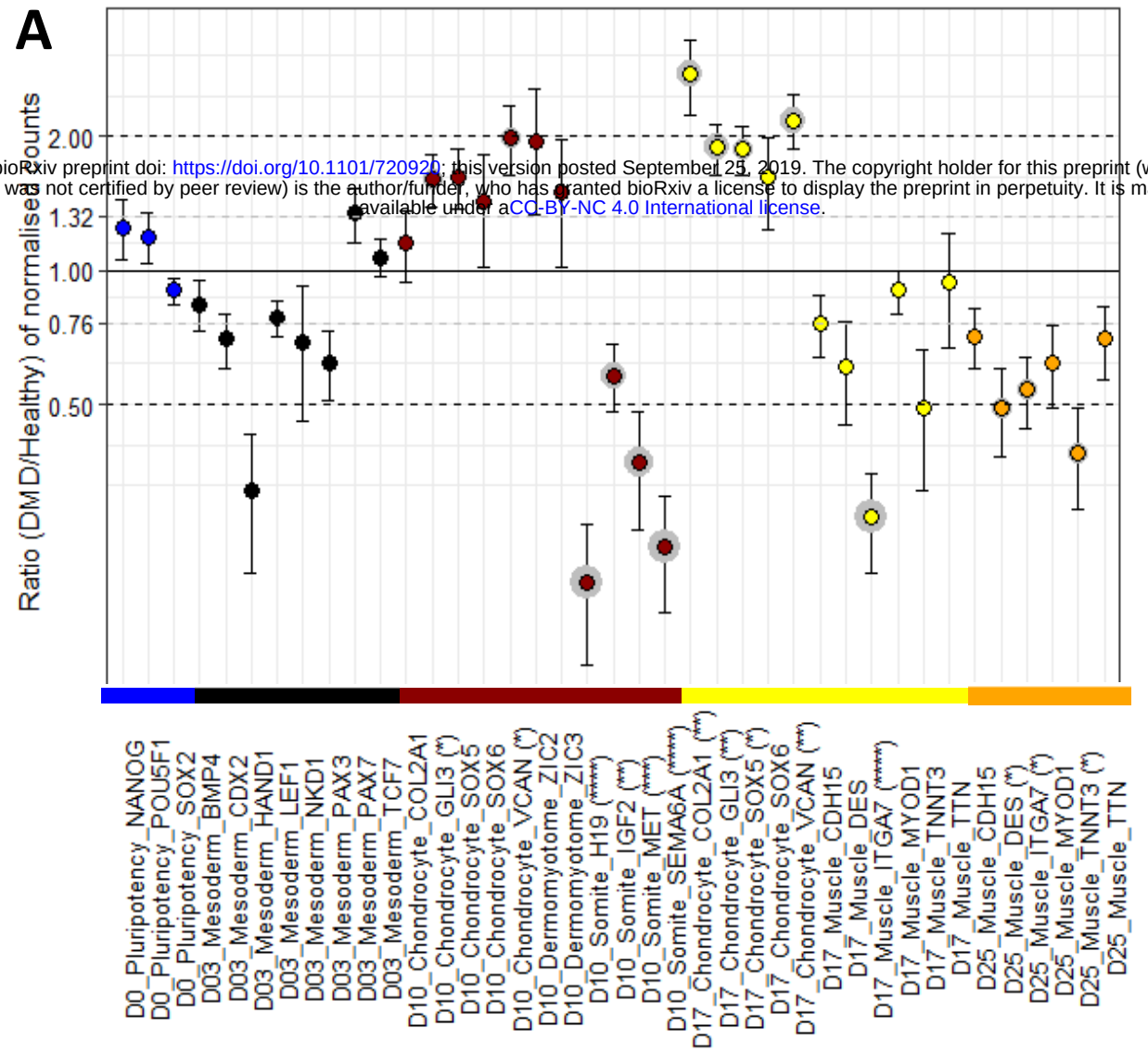

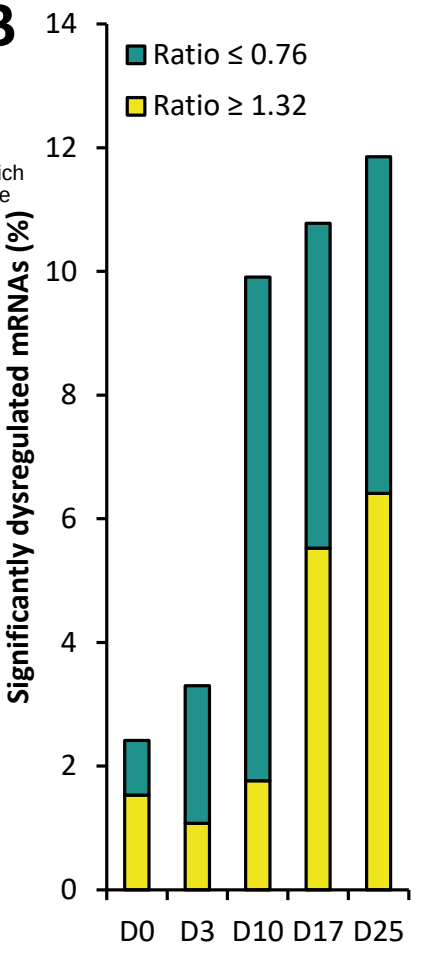

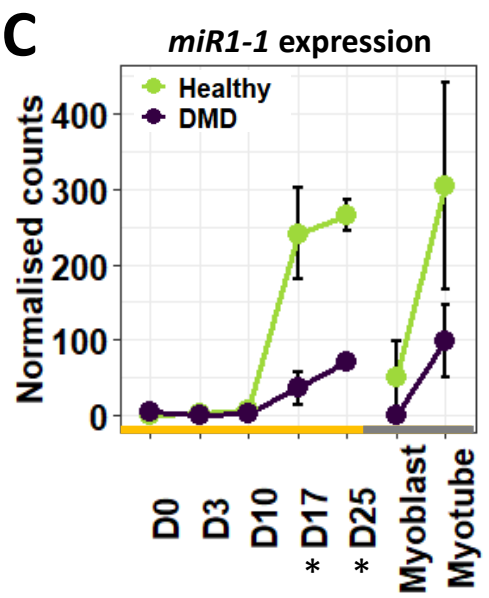

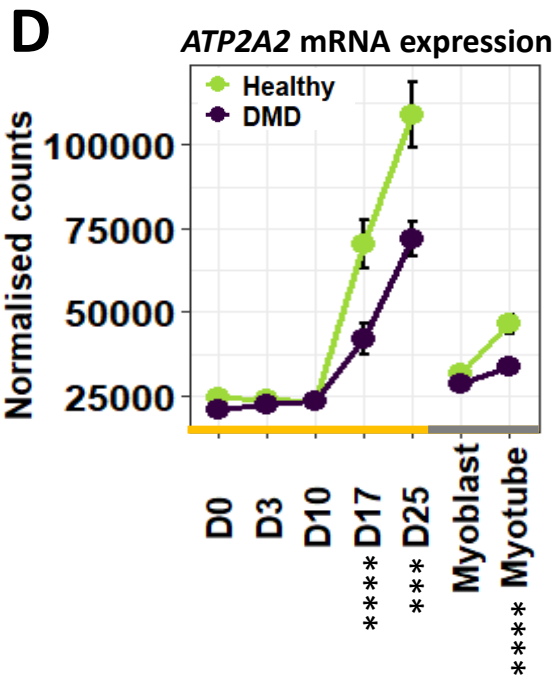

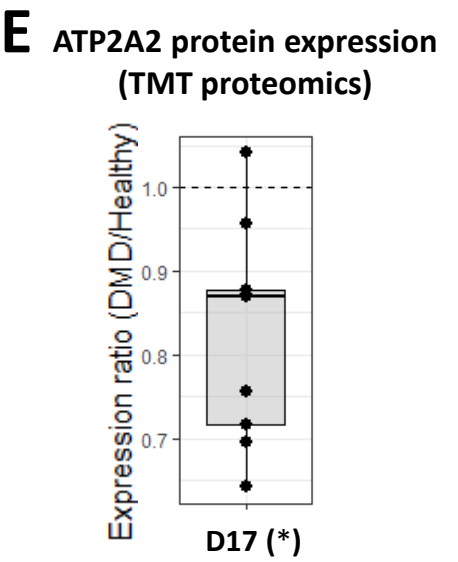

Figure 3

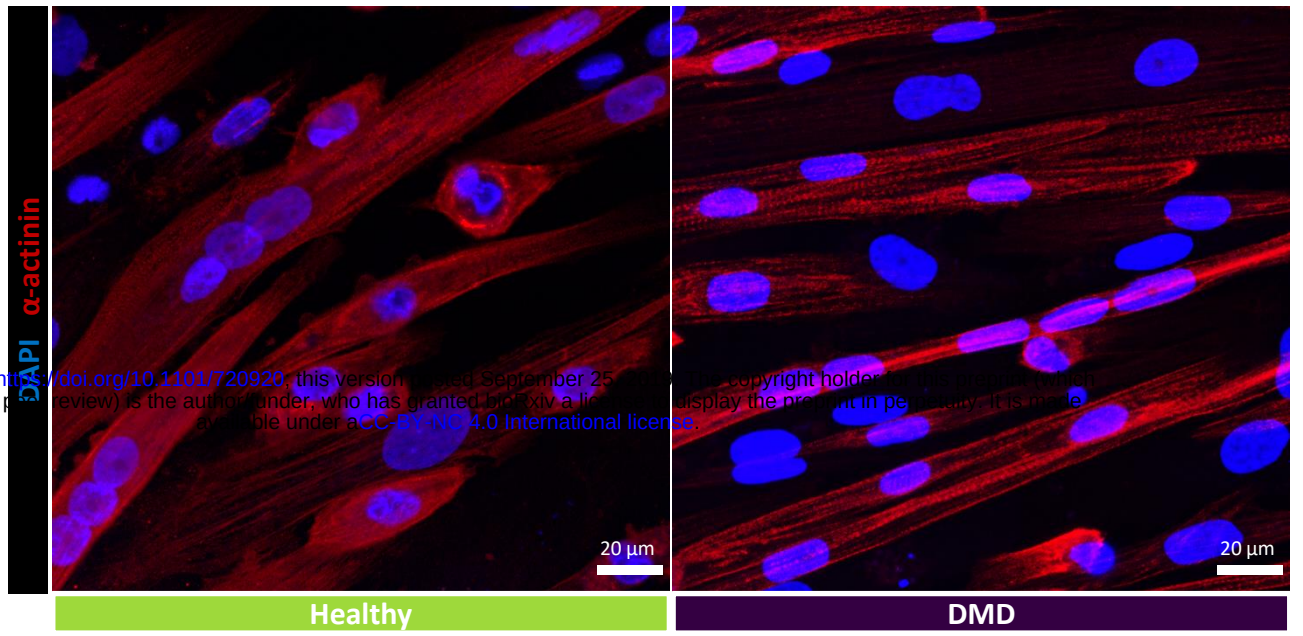

Figure 4

A

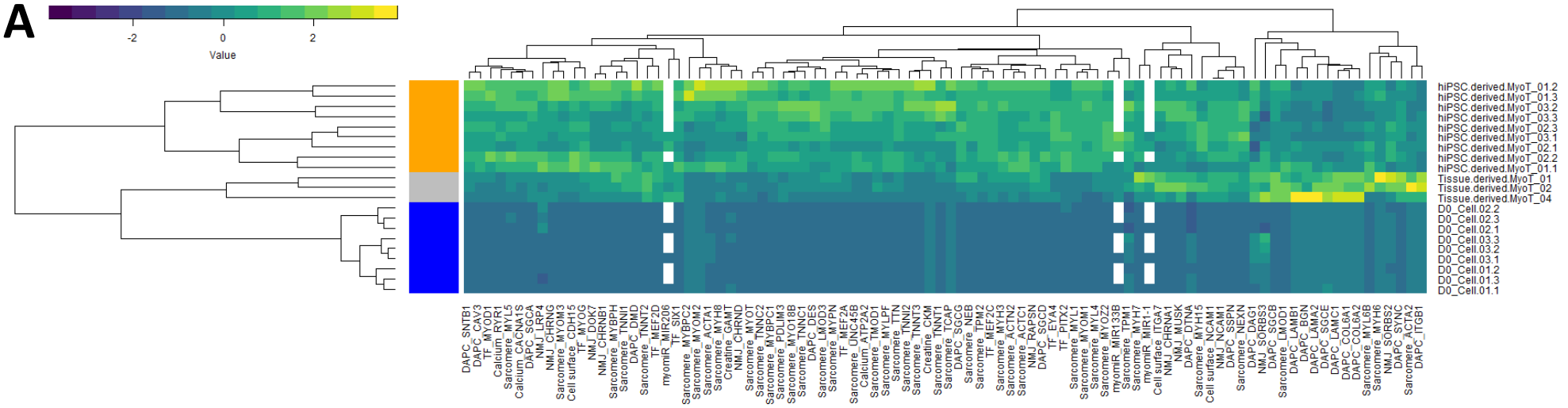

B

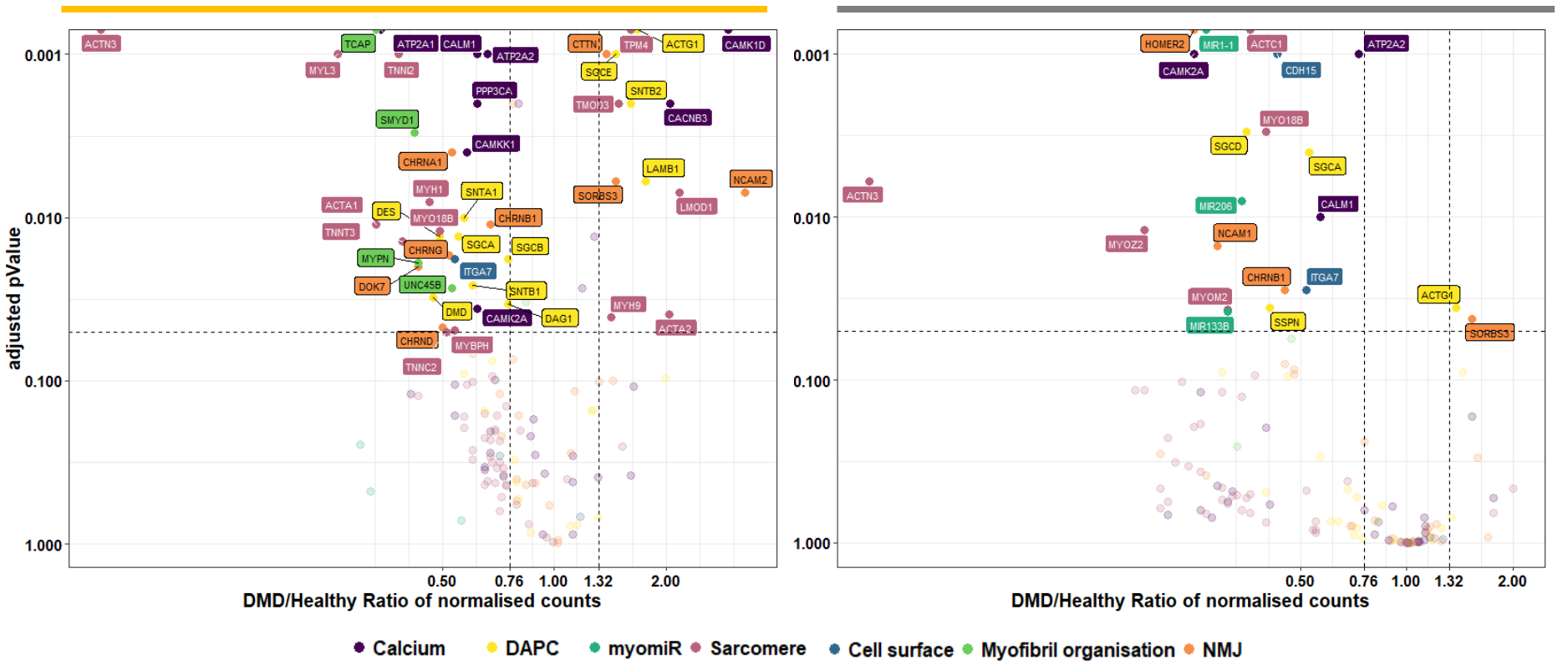

Figure 5

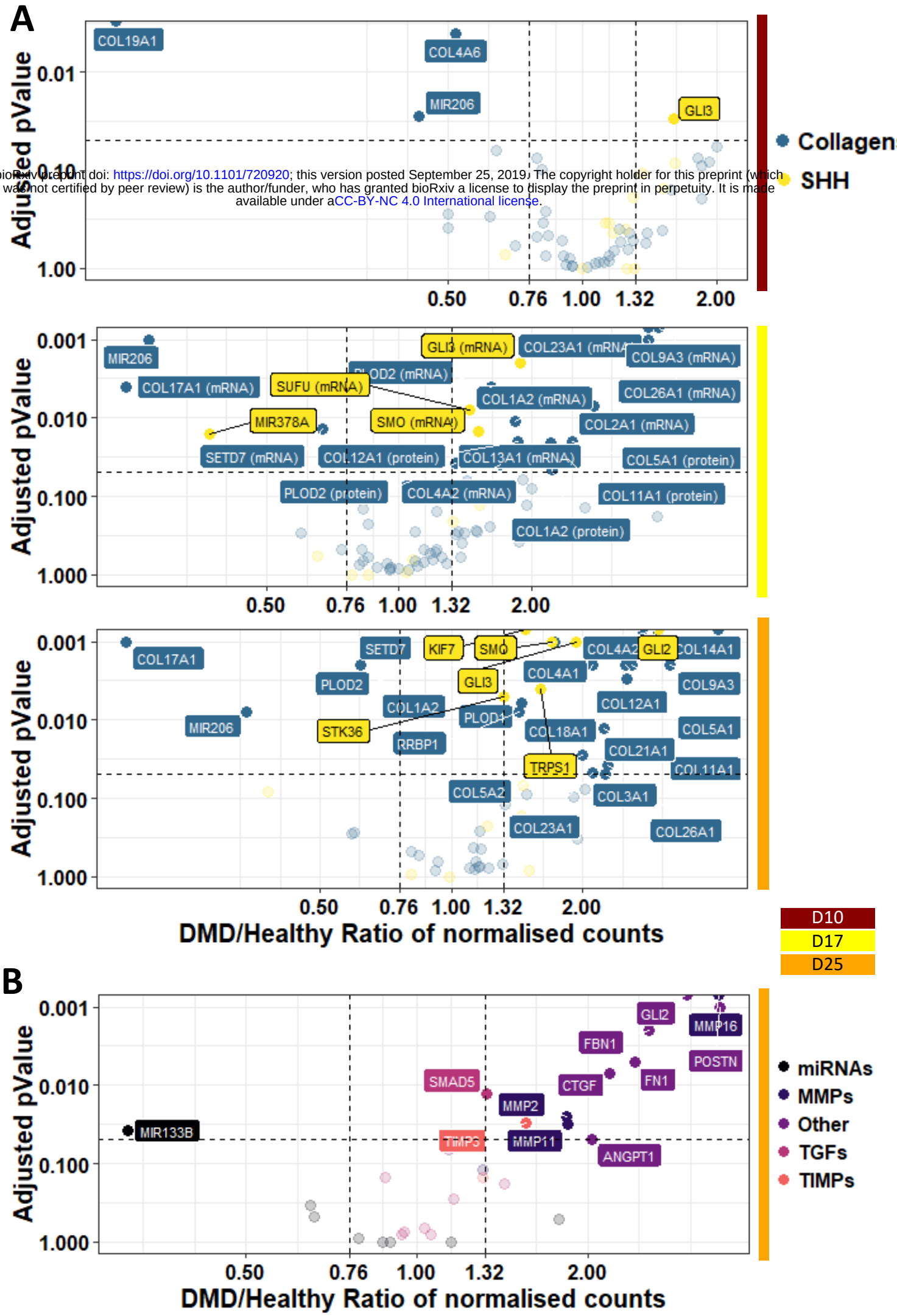

Figure 6

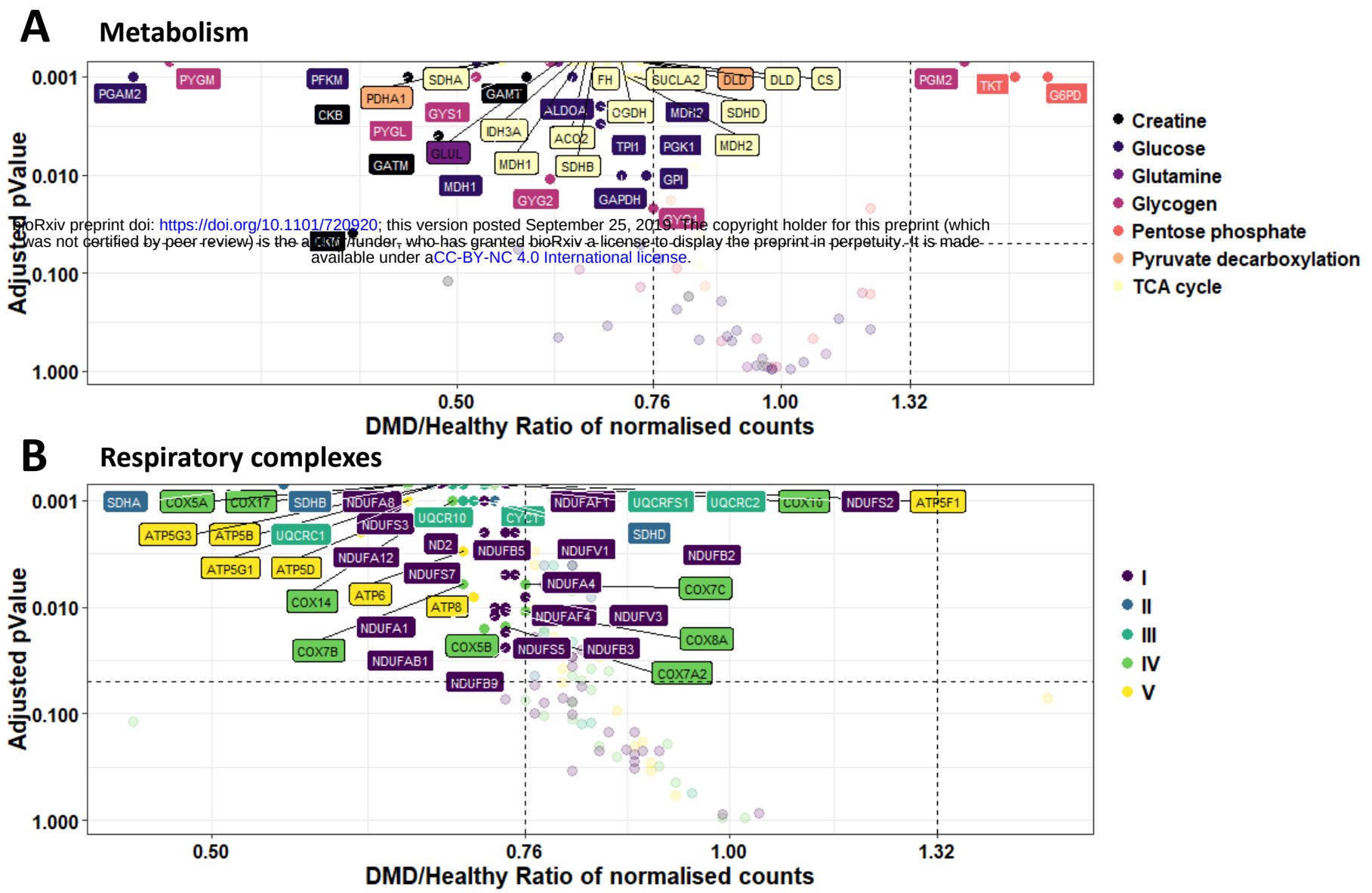

Figure 7